

REVIEW ARTICLE

Zero Temperature Numerical Studies of Multiband Lattice Models of Strongly Correlated Electrons

Yong-Qiang Wang¹, Hai-Qing Lin^{1,*} and J. E. Gubernatis²

¹ *Department of Physics and the Institute of Theoretical Physics, The Chinese University of Hong Kong, Shatin, N.T., Hong Kong SAR.*

² *Theoretical Division, Los Alamos National Laboratory, Los Alamos, NM 87545 USA.*

Received 25 January 2006; Accepted (in revised version) 8 May, 2006

Abstract. Relative to single-band models, multiband models of strongly interacting electron systems are of growing interest because of their wider range of novel phenomena and their closer match to the electronic structure of real materials. In this brief review we discuss the physics of three multiband models (the three-band Hubbard, the periodic Anderson, and the Falicov-Kimball models) that was obtained by numerical simulations at zero temperature. We first give heuristic descriptions of the three principal numerical methods (the Lanczos, the density matrix renormalization group, and the constrained-path Monte Carlo methods). We then present generalized versions of the models and discuss the measurables most often associated with them. Finally, we summarize the results of their ground state numerical studies. While each model was developed to study specific phenomena, unexpected phenomena, usually of a subtle quantum mechanical nature, are often exhibited. Just as often, the predictions of the numerical simulations differ from those of mean-field theories.

Key words: Lanczos method; density matrix renormalization group; constrained-path Monte Carlo; three-band Hubbard model; periodic Anderson model; Falicov-Kimball model

Contents

1	Introduction	576
2	Numerical methods	577
3	Basic models	589
4	Numerical results	596
5	Summary	608

*Correspondence to: Hai-Qing Lin, Department of Physics and the Institute of Theoretical Physics, The Chinese University of Hong Kong, Shatin, N.T., Hong Kong SAR. Email: hqlin@sun1.phy.cuhk.edu.hk

1 Introduction

As a tool for understanding the properties of strongly correlated electron systems, numerical methods are both an opportunity and a challenge. They are an opportunity because in only a few cases are the simplest models of such systems exactly solvable. By producing very accurate solutions and thereby filling the gap between an exact solution and an uncontrolled approximation, these methods are thus an importantly useful way to advance the understanding of the properties of these models. What has been significant is their frequent revelations of unexpected and important new physics that standard perturbation and mean-field theories unfortunately often miss. The challenge is finding numerical algorithms that work well.

In this review we will be concerned only with results produced by three current common methods for producing the zero temperature energy and wavefunction of certain strongly correlated electron models. In general, there are three classes of zero temperature numerical methods: Krylov space [1,2], density-matrix renormalization group (DMRG) [3], and projector Monte Carlo methods. From the wavefunction that each estimates, a variety of physical properties, other than the energy, are easily calculated.

The Monte Carlo method allows the largest system sizes to be studied but with an accuracy that is in general several orders of magnitude less than the other two. The infamous fermion sign problem [4], manifested by the statistical variance of the numerical solution becoming exponentially large as the size of the system simulated becomes large, plagues these algorithms. The DMRG method, particularly in one dimension, allows the study of the next largest system sizes with a high degree of accuracy. For just the basic qualitative picture of the models's possible phases, as opposed to extrapolating its properties to the thermodynamics limit, a particular Krylov space method, the Lanczos method [1,2], is often the method of choice. Although often called the exact diagonalization method (ED), it actually only produces a variational upper bound to the ground state energy of the model. The accuracy of the method however is usually outstanding, being nearly full floating point precision.

In this review we will only present recent results of zero temperature numerical studies of the three-band Hubbard, periodic Anderson, and Falicov-Kimball models. All three are multiband models. The three-band Hubbard obtains multiband stature from having three single orbital atoms per unit cell. It is inherently two-dimensional, being proposed to model the CuO_2 planes in high temperature superconductors. For this model the numerical simulations have focused on the behavior the d -wave pairing correlation function as a function of the model's parameter. Here, the results are obtained by use of a particular projector Monte Carlo method, the constrained-path Monte Carlo method (CPMC) [5-7]. This method is also the primary tool for the results presented for the periodic Anderson model. The focus of these results will be magnetic properties, particularly its ferromagnetic properties. The model which shows the most novel physics is the Falicov-Kimball model. For the simplest version of the model, a combination of analytic work using strong coupling theory and numerical work using the ED and CPMC methods, has demonstrated the

existence of fixed and mixed valence phases with the mixed valence phase being one of either staggered orbital ordering or one with a chiral and electronic ferroelectric phase coexisting [8–10].

We will begin by giving brief descriptions of the Lanczos, density-matrix renormalization group, and constrained-path Monte Carlo methods. We will describe their basic strategies to highlight their differences. Detailed descriptions of each are readily available elsewhere [6, 7, 11, 12]. Next, in Section 3, we will describe the three models. Here we will also describe the various physical quantities that have been the focus of computations. In Section 4, we will summarize the principal zero temperature numerical results obtained for these models. Lastly, in Section 5, we conclude with some suggestions for some needed improvements in the numerical methods and some opportunities for new numerical studies.

2 Numerical methods

2.1 Lanczos

The Lanczos method is an iterative method to compute the eigenvalues and eigenvectors of large, sparse, real, symmetric matrices. It involves the partial tridiagonalization of the large matrix and is marked by the extremal eigenvalues, that is, the smallest and largest eigenvalues, of this much smaller matrix rapidly converging to those of the much larger one.

The method has enjoyed considerable use in studying the physics of one-band electronic models, such as the Hubbard [13] and t - J models [14], and quantum spin models, such as the Heisenberg model. Its use is limited by the size of computer memory, not spatial dimension. In particular, the size of the largest matrix that can be studied is determined by the ability to store in computer memory 2 or 3 vectors of the order of the Hamiltonian matrix. (For the problems at hand this matrix is not stored but computed on-the-fly.) This vector size in turn is determined by the number of lattice sites and the number electrons. For a N site periodic Anderson model with a $S_z = \frac{1}{2}|N_\uparrow - N_\downarrow|$ ground-state, this size is

$$M = \frac{(2N)!}{N_\uparrow!(2N - N_\uparrow)!} \times \frac{(2N)!}{N_\downarrow!(2N - N_\downarrow)!}.$$

For a 6 site lattice with $N_\uparrow = N_\downarrow = 3$, $M = 48200$; with $N_\uparrow = N_\downarrow = 6$, $M = 853776$. In general, the number of sites that can be studied for a two band model is half that of a one-band model; for a three-band model, it is one third. Typically, symmetries of the model Hamiltonian are used to block diagonalize the Hamiltonian matrix, and then the method is applied to each relevant block. The most frequently used symmetry is translational symmetry. In general, it reduces the size of the Hilbert space and hence the size of the matrices by N . Other symmetries commonly used are the point group symmetries of the lattice. They may, for example, allow one to study the ground state as a function of S_z . Sometimes one can also use spin reflection symmetry.

In one dimension, the energy for the largest chain possible for one-band models is on the verge of being extensive. The number of sites that can be studied is however independent of the spatial dimension. In dimensions higher than one, finite-size effects become more apparent even for one-band models. As the mathematics of the Lanczos method is well described elsewhere [1,2] and a tutorial article [11] describing its implementation for electron lattice and quantum spin model exists, we will only describe its most important features.

To understand the workings of the method the concept of an invariant subspace is important. First, a subspace is defined as the set of all n -vectors that can be written as a linear combination of the set $S = \{s_1, s_2, \dots, s_m\}$. If A is a symmetric matrix, then the subspace is said to be invariant under A if for any vector x in the subspace, the vector Ax is also in the subspace. If $Q = \{q_1, q_2, \dots, q_m\}$ is any basis of an invariant subspace under A , arranged in the form of the n by m matrix Q whose columns are the n -vectors q_i , then the action of the n by n matrix A on Q is just to form a new n by m matrix AQ whose columns are a linear combination of the columns of Q . A m by m matrix C can represent this combination and expresses the restriction of A to this subspace

$$AQ = QC. \tag{2.1}$$

The utility of this concept is the following: If (λ, y) is an eigenpair of C , then

$$\begin{aligned} Cy &= \lambda y, \\ QCy &= \lambda Qy, \\ A(Qy) &= \lambda(Qy), \end{aligned} \tag{2.2}$$

meaning that λ is also an eigenvalue of A and Qy is the corresponding eigenvector. Thus, eigenpairs of a very large matrix can be found from those of a much smaller one if the space spanned by Q is invariant under A . Knowing this space however is equivalent to knowing the solution of the eigenvalue problem, but an approximate space can often be constructed thereby enabling good estimates of some eigenpairs.

The Lanczos method does this by approximating C by a tridiagonal matrix

$$T = \begin{bmatrix} \alpha_1 & \beta_1 & & \dots & & 0 \\ \beta_1 & \alpha_2 & & \ddots & & \vdots \\ & & \ddots & \ddots & & \\ \vdots & & & \ddots & \ddots & \beta_{m-1} \\ 0 & \dots & & \beta_{m-1} & & \alpha_m \end{bmatrix}. \tag{2.3}$$

As a subspace, it chooses the one spanned by the Krylov sequence

$$Q = (b, Ab, A^2b, \dots, A^{m-1}b), \tag{2.4}$$

where b is an arbitrary vector. This sequence approximates an invariant subspace under A . The argument is: Under A , the vectors $Ab, A^2b, \dots, A^m b$ are all in the Krylov space

except for the last one. It can be shown that $A^{m-1}b$ converges to an eigenvector of A if m is sufficiently large, so $A^m b$ is approximately proportional to $A^{m-1}b$ and hence is almost in the Krylov space. Thus, to a very good approximation, the Krylov space for $m < n$ is an invariant subspace of A .

The α 's and β 's are determined from the recursion relation

$$Aq_i = \beta_{i-1}q_{i-1} + \alpha_i q_i + \beta_{i+1}q_{i+1}, \quad (2.5)$$

which follows from Eq. (2.1) with T in Eq. (2.3) replacing C . To find the lowest eigenvalue λ_1 , a reasonable guess b to the ground state wavefunction is made, and the α 's and β 's are determined iteratively. At the end of each iteration, a successively larger tridiagonal matrix is generated whose eigenpairs are obtained with a conventional tridiagonal solver [1]. The iteration is continued until λ_1 converges to the required accuracy.

The recursion relation, Eq. (2.5), preserves the symmetries in the initial guess q_0 . This feature enables the separation of the eigenvalues into different sub-spaces of the Hamiltonian, for example, different values of the momenta k . Thus, not only one can determine the ground state energy accurately, but also the energies of some low lying excited states. Additionally, one will always find the lowest eigenvalue in the subspace where iteration started, as long as the initial state q_0 lies in it. However, the efficiency of the method and the accuracy of the smallest eigenvalue (the ground state) depend on the gap between it and the next lowest state. The larger the gap, the faster and more accurately the method converges to the lowest eigenvalue. For a non-interacting problem with the matrix size being $M = 2N$, this gap is typically a finite size effect and can be large. When the interaction is turned on, the gap can become very small unless the model has a true gap.

This closing of the pseudo-gap sometimes makes determining the ground state energy of the interacting problem difficult. In practice, we try different initial states with different symmetries. When number of iteration is larger than 200 and the accuracy is only of the order 10^{-7} , we consider the iteration unsatisfactory and try the new one. On the other hand, to avoid finding a solution for a local minimum instead of the ground state, many Lanczos iterations are executed with a random selection of initial states.

2.2 Density matrix renormalization group

Today, the density matrix renormalization group (DMRG) method is the most widely used technique for finding the ground state properties of one-dimensional lattice models of interacting electrons and quantum spins. At the same time, it is still under improvement. In practice, the method is most effective in one dimension for models with open boundary conditions and short-ranged interactions. Recently, the DMRG has enjoyed a surge of new interest by quantum information theorists. They are interested in the relationship between the product basis functions assumed in the DMRG method and the entanglement of quantum many body states. Many of the recent improvements being proposed for the DMRG come from these interests and their emerging insights. Several slightly different

approaches to its implementation exist, and these are referenced in a recent extensive review [12] that referenced many other reviews. Here, we will focus on general issues aimed at contrasting it with the Lanczos algorithm. We will start by noting the different uses of an invariant subspace and then sketch one possible way to implement the method.

At its core, the DMRG uses an ED method, such as the Lanczos or the Davidson method [15, 16], to find the ground state of a large sparse matrix. In contrast to these ED methods that use a Hamiltonian of fixed lattice size at each stage of the iteration, the DMRG method iteratively increases the lattice size defining the Hamiltonian. At each iteration this larger lattice Hamiltonian is given to a ED method which returns the ground state wavefunction from which the density matrix of the system is computed. The eigenvectors of the largest eigenvalues of this matrix, and not those of Hamiltonian matrix, become the truncated basis represented by the matrix Q used to restrict the Hamiltonian to a smaller basis. In the DMRG restriction, the columns of Q are orthonormal so that $Q^T Q = I$. From Eq. (2.1), this implies $C = Q^T H Q$. There are several justifications given for this strategy [12]: It leads to an optimization of the expectation values, wavefunction, and entanglement of the estimated solution relative to the exact result. It also leads to a variational estimate of the ground state energy.

To sketch the workings of the method, we will suppose we have a one-band Hamiltonian H , the Hubbard model, for instance, defined in one dimension with open boundary conditions plus hopping amplitudes and Coulomb interactions restricted to neighboring sites. We can write this Hamiltonian as

$$H = H_S + H_{\bullet\bullet} + H_E. \quad (2.6)$$

If the lattice has N sites, H_S is that part of the H defined on the first N_S sites going from left to right; it is usually called the system S . H_E is the part of H defined on the last N_E sites; it is called the environment E . The number of sites satisfies $N = N_S + N_E$. The last piece $H_{\bullet\bullet}$ is the interaction between these two systems. With $i = N_S$ it has terms like $c_i^\dagger c_{i+1} + c_{i+1}^\dagger c_i$. We will also assume that the size M of the basis needed for the number of sites and the number of electrons is the the largest possible for our ED method. If M_S and M_E are the basis sizes for the system and environment, then $M = M_S M_E$. Using this break-up of H , we find the ground state wavefunction which we write as

$$|\Psi_0\rangle = \sum_{\sigma, \epsilon} A_{\sigma\epsilon} |\sigma\epsilon\rangle = \sum_{\sigma, \epsilon} A_{\sigma\epsilon} |\sigma\rangle |\epsilon\rangle, \quad (2.7)$$

where the $|\sigma\rangle$ states refer to S ; the $|\epsilon\rangle$, to E .

For electron lattice models, associated with each site is a local set of basis states $\{|s\rangle\}$ where $s = 1, 2, \dots, M_{site}$. For a generic one-band model, $M_{site} = 4$, and $|1\rangle$ is the state with no electron; $|2\rangle$, one up electron; $|3\rangle$, one down electron; and $|4\rangle$, double occupancy. In Eq. (2.11), the set of system states $\{|\sigma\rangle\} = \{|s_1\rangle, |s_2\rangle, \dots, |s_{N_S}\rangle\}$ where $s_i = 1, 2, \dots, M_{site}$. Alternatively, $\{|\sigma\rangle\} = \{|Ss\rangle\} = \{|S\rangle|s\rangle\}$ where $S = 1, 2, \dots, M_S/M_{site}$ and $s = 1, 2, \dots, M_{site}$. Similar definitions hold for the environment. reduced density matrices

for S and E

$$\rho_{\sigma\sigma'}^S = \sum_{\epsilon} A_{\sigma\epsilon} A_{\sigma'\epsilon}, \quad \rho_{\epsilon\epsilon'}^E = \sum_{\sigma} A_{\sigma\epsilon} A_{\sigma\epsilon'} \quad (2.8)$$

are computed and a conventional eigensolver is used to find the M_S/M_{site} and M_E/M_{site} eigenvectors corresponding to the the M_S/M_{site} and M_E/M_{site} largest eigenvalues of ρ_S and ρ_E . These eigenvectors define Q_E and Q_S which are then used to restrict the system to the reduced basis

$$Q_S^T H_S Q_S \rightarrow H_S, \quad Q_E^T H_E Q_E \rightarrow H_E. \quad (2.9)$$

Similar restrictions of the matrix elements of the operators defining the Hamiltonian for the S and E sites are also made and stored. They are needed to build the Hamiltonian to a larger lattice size.

The lattice size is grown by adding two sites. The Hamiltonian is now written as

$$H = H_S + H_{S\bullet} + H_{\bullet\bullet} + H_{\bullet E} + H_E. \quad (2.10)$$

Now $N = N_S + N_E + 2$ but the value of M is unchanged. The new pieces of H refer to these additional two sites. $H_{S\bullet}$ has contributions coming from S and the site $i = N_S + 1$ to the right of S ; $H_{\bullet E}$, from E and the site $i + 1$ to the left of E . In the original representation, these Hamiltonians would have terms like $c_{i-1}^\dagger c_i$, n_i , $c_{i+1}^\dagger c_{i+2}$, and n_{i+1} . Matrix elements of operators referring to sites i and $i + 1$ are expressed in the original $\{|s\rangle\}$ basis. Those for sites $i - 1$ and $i + 2$ are in the restricted $\{|S\rangle\}$ and $\{|E\rangle\}$ bases. The last piece $H_{\bullet\bullet}$ is now the interaction between these two additional sites. It has terms like $c_i^\dagger c_{i+1} + c_{i+1}^\dagger c_i$.

Giving this Hamiltonian to an ED method, we find the ground state wavefunction which we again write as

$$|\Psi_0\rangle = \sum_{\sigma,\epsilon} A_{\sigma\epsilon} |\sigma\rangle\epsilon\rangle. \quad (2.11)$$

The σ states now refers to S plus the additional site; the ϵ state, to E plus the additional site. In particular $\{|\sigma\rangle\} = \{|S\rangle|s\rangle\}$ and $\{|\epsilon\rangle\} = \{|E\rangle|s\rangle\}$. The restriction is performed

$$Q_S^T H_S Q_S \rightarrow H_S, \quad Q_E^T H_E Q_E \rightarrow H_E, \quad (2.12)$$

the matrix elements of the operators are restricted, and the process repeated. An estimate of an observable X is obtained from

$$\langle X \rangle = \frac{\langle \Psi_0 | X | \Psi_0 \rangle}{\langle \Psi_0 | \Psi_0 \rangle}. \quad (2.13)$$

Typically, $N_S = N_E$ and this process is repeated until some maximum lattice length is reached. The physical system will usually have reflection symmetry between the two halves which eliminates the need to compute system and environment components independently. The procedure just described is called the infinite-system algorithm. Its steps are illustrated in Fig. 1. Often, more satisfying results are obtained by executing the finite-system algorithm after the infinite-system algorithm is completed.

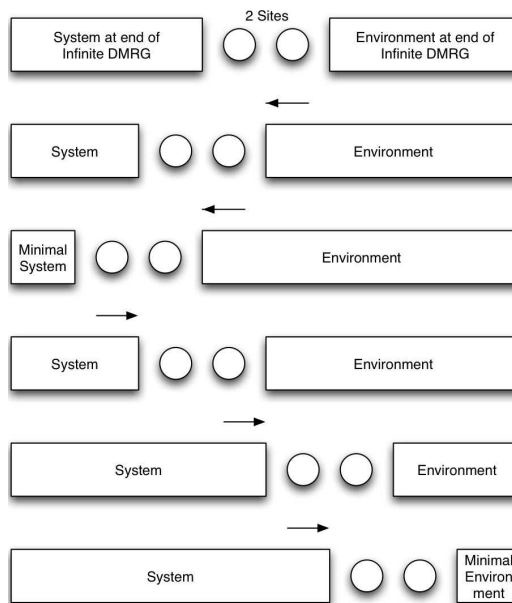


Figure 1: Fundamental construction in the infinite-system DMRG using systems and environment blocks plus two sites (after [12]).

In the finite-system algorithm, N is fixed and a small number of sweeps are executed. A sweep has two stages. In one stage, right to left (environment growth), a site is added to E and removed from S until the size of S reaches the minimal value where all the matrix elements of H_S are known exactly. This size is usually the value at the starting point. The second stage is now left to right (system growth): A site is removed from E and added to S until the starting size of E is reached. Restriction is applied only to the growing system. The shrinking system is constructed from the matrix elements of the restricted operators generated and stored during the execution of the infinite system algorithm. The process is depicted in Fig. 2.

There are multiple reasons for the need of the finite-system algorithm. Most relevant for electron models is the need to keep the electron density constant as the lattice size grows by "injecting" electrons into the system and environment. If haphazard, this injection can lead to a electronic distribution inadequately relaxed. The sweeps of the finite-system algorithm provide the relaxation. In general, the finite-system algorithm reduces the likelihood of the solution representing a metastable state as opposed to the true ground state.

The Hamiltonian break-ups in Eqs. (2.6) and (2.10) are more symbolic than precise. To be more precise, H_S in Eq. (2.6), for example, should be written as $H_S \otimes I_E$ where I_E is the identity in the environment basis, while in Eq. (2.10) it should be written as $(H_S \otimes I_\bullet) \otimes I_E$ where I_\bullet is the identity in the local basis. This structure makes the break-up of the Hamiltonian consistent with the direct product expressions (2.7) and (2.11) for the

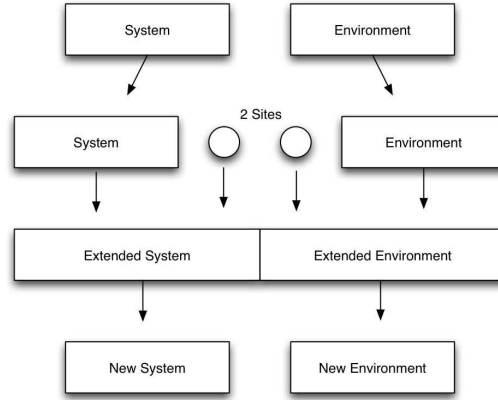


Figure 2: Fundamental construction in the finite-system DMRG (after [12]).

wavefunction. In terms of the matrices A and B , a direct product is defined by

$$A \otimes B = \begin{bmatrix} A_{11}B & A_{12}B & A_{13}B & \cdots \\ A_{21}B & A_{22}B & A_{23}B & \cdots \\ A_{31}B & A_{32}B & A_{33}B & \cdots \\ \vdots & \vdots & \vdots & \ddots \end{bmatrix}. \quad (2.14)$$

If A and B are 2 by 2 matrices, the direct product matrix is

$$A \otimes B = \begin{bmatrix} A_{11}B_{11} & A_{11}B_{12} & A_{12}B_{11} & A_{12}B_{12} \\ A_{11}B_{21} & A_{11}B_{22} & A_{12}B_{21} & A_{12}B_{22} \\ A_{21}B_{11} & A_{21}B_{12} & A_{22}B_{11} & A_{22}B_{12} \\ A_{21}B_{21} & A_{21}B_{22} & A_{22}B_{21} & A_{22}B_{22} \end{bmatrix}. \quad (2.15)$$

It is inefficient to express H other than in the direct product form. To do otherwise requires significant computer memory and significantly more computer time. Such products have the useful relations

$$(A_1 \otimes B_1)(A_2 \otimes B_2) = (A_1 B_1) \otimes (A_2 B_2), \quad (2.16a)$$

$$(A \otimes B)^{-1} = B^{-1} \otimes A^{-1}, \quad (2.16b)$$

$$(S^{-1} \otimes T^{-1})(A \otimes B)(S \otimes T) = (S^{-1}AS) \otimes (T^{-1}BT). \quad (2.16c)$$

This means that for the ground state in Eq. (2.11) the computation of a quantity such as

$$\begin{aligned} \langle \sigma' \epsilon' | H_S | \Psi_0 \rangle &= \sum_{\sigma, \epsilon} A_{\sigma \epsilon} \langle \sigma' \epsilon' | H_S | \sigma \epsilon \rangle \\ &= \sum_{\sigma} A_{\sigma \epsilon'} \langle \sigma' | H_S | \sigma \rangle \\ &= \sum_S A_{S \sigma' \epsilon'} \langle S' | H_S | S \rangle \end{aligned} \quad (2.17)$$

reduces to a matrix-vector multiplication

$$\langle S' s' \epsilon' | H_S | \Psi_0 \rangle = \sum_S [H_S]_{S' S} A_{S s' \epsilon'} \quad (2.18)$$

in a space reduced with respect to that of σ , with only the matrix elements of $\langle \sigma' \epsilon' | H_S | \Psi_0 \rangle$ in this reduced space needing computation. Such products scale as the order of the matrix squared, so the computation reduction is significant and even more significant for other examples.

If a multiband model were considered, instead of the one-band one just discussed, M_{site} would be much larger which means the bases sizes for the system and environment would be smaller and a reduction in accuracy is expected. If longer-ranged hoppings or interactions were added, additional pieces would appear in the break-up of the Hamiltonian. Handling them would require more computer time and memory. The increase in memory requirements means the bases sizes for the system and environment would be smaller and a reduction in accuracy is again expected. Similar issues are generated in higher dimensions or with periodic boundary conditions. Still, the DMRG method is capable of treating larger multiband models in one and two-dimensions than is possible with the ED method alone. To date, the DMRG has been underutilized in these contexts.

One of the new developments in the DMRG method is a very recent proposal by White [17] that adds one site at a time instead of two. Reductions by factors of two to four in computer time and memory are reported, along with a reduction in tendency of being trapped in metastable states. Most of the excitement about significant improvement in the DMRG have come from proposals rooted in quantum information theory that replace the direct-product space representation of the wavefunction by a matrix-product representation [12]. States in this representation are often a better representation of the actual ground state of systems in one or more dimensions and accordingly have promise of increasing the range of practical uses of the method.

2.3 Constrained-path Monte Carlo

As does the ED method, ground state quantum Monte Carlo methods use an iterative procedure to project the ground state energy and wavefunction from a suitably chosen starting point. In contrast to this deterministic method, a Monte Carlo procedure is used to estimate the values of the implied integrations (summations) present at each step in the iteration. The eventual result is the generation of a large number of successive “samples” of the the solution instead of one specific estimate. The Monte Carlo solution is not the wavefunction itself but averages of various physical quantities computed from samples drawn from that wavefunction.

Various vastly different looking techniques fall under the rubric “quantum Monte Carlo.” We will be concerned exclusively with the constrained-path Monte Carlo method [5–7]. It belongs to a class of projector Monte Carlo methods that includes the auxiliary-field [18, 19] and lattice fixed node methods [20]. The auxiliary-field method possess a sign

problem. In many respects it is a parent of the lattice fixed-node and constrained-path methods. The latter two eliminate the sign problem by making an approximation but differ in the manner in which this approximation is made and in the space in which the random walk is executed. We are unaware of any application of the lattice fixed-node method to multiband models.

The constrained-path method is a Markov chain Monte Carlo method. This type of Monte Carlo is defined by a transition probability P_{ij} for going from state j to state i and some initial distribution $p_i^{(0)}$. The chain is generated iteratively by

$$p_k^{(i+1)} = \sum_j P_{kj} p_j^{(i)}. \tag{2.19}$$

Eventually, under very general conditions on P_{ij} , a fixed point condition is reached

$$p_j = \sum_k P_{kj} p_j, \tag{2.20}$$

and it becomes possible to “sample” subsets of the allowed states j distributed by p [21]. In most of statistical mechanics a specific fixed-point distribution is required, usually the Boltzmann distribution. The power of the famous Metropolis Algorithm [22] is being a means to specify a simple P that samples from a specific p . In the current applications, we however know P and endeavor to determine p . This distribution will turn out to be the ground-state wavefunction. Hence, the quantum Monte Carlo method will generate many samples of the ground state wavefunction. For fermions, the sign problem means this function p will not be everywhere positive and hence not a true distribution. The Monte Carlo method is executed with adjustments.

As a first step, we place our quantum ground state problem in the form of Eq. (2.20). We accomplish this by transforming the time-dependent Schrödinger’s equation into an imaginary-time one,

$$i \frac{\partial |\Psi\rangle}{\partial t} = H |\Psi\rangle \xrightarrow{it \rightarrow \tau} \frac{\partial |\Psi\rangle}{\partial \tau} = -H |\Psi\rangle, \tag{2.21}$$

which has the formal solution

$$|\Psi(\tau)\rangle = e^{-\tau H} |\Psi(0)\rangle. \tag{2.22}$$

One observes that if

$$|\Psi(0)\rangle = a_0 |\Psi_0\rangle + a_1 |\Psi_1\rangle + \dots,$$

with

$$H |\Psi_i\rangle = E_i |\Psi_i\rangle, \quad E_i \leq E_{i+1}, \tag{2.23}$$

then

$$|\Psi(\tau)\rangle \xrightarrow{\tau \rightarrow \infty} a_0 e^{-\tau E_0} |\Psi_0\rangle + a_1 e^{-\tau E_1} |\Psi_1\rangle + \dots. \tag{2.24}$$

This limit can be obtained iteratively from

$$|\Psi(\tau + \Delta\tau)\rangle = U(\tau + \Delta\tau, \tau) |\Psi(\tau)\rangle, \tag{2.25}$$

where

$$U(\tau + \Delta\tau, \tau) = e^{-\Delta\tau(H-E_0)}. \tag{2.26}$$

After many iterations,

$$\begin{aligned} |\Psi(\tau + \Delta\tau)\rangle &= U(\tau + \Delta\tau, \tau) |\Psi(\tau)\rangle \\ &= a_0 |\Psi_0\rangle + a_1 e^{-\Delta\tau(E_1-E_0)} |\Psi_1\rangle + \dots \\ &\approx a_0 |\Psi_0\rangle. \end{aligned} \tag{2.27}$$

Hence the fixed-point condition is

$$|\Psi(\tau)\rangle = U(\tau + \Delta\tau, \tau) |\Psi(\tau)\rangle. \tag{2.28}$$

Some good guesses, E_T and $|\Psi_T\rangle$, are used for E_0 and the starting state $|\Psi(0)\rangle$.

Next we note that any many-fermion wavefunction can be written as a linear combination of Slater determinants. The constrained-path method does this via

$$|\Psi_0\rangle = \sum_{\phi} A_{\phi} |\phi\rangle, \tag{2.29}$$

where the sum is over the space of all possible Slater determinants. Any one determinant will be of the form

$$|\phi\rangle = b_1^{\dagger} b_2^{\dagger} \dots b_N^{\dagger} |0\rangle, \tag{2.30}$$

where

$$b_j^{\dagger} = \sum_i c_i^{\dagger} B_{ij}. \tag{2.31}$$

The matrix B , which in general is rectangular, defines operators that create and destroy electrons in new orbitals defined relative to some prior set. This set is usually referenced to the operators defining the original Hamiltonian. Because our Hamiltonians in general exhibit time reversal invariance, we can choose our ground state to be real and choose the phase of the ground state so that the A_{ϕ} are all positive. These coefficients then define the p that the Monte Carlo procedure wants to sample. The sign problem arises because the Monte-Carlo-based iteration produces states with not all the A_{ϕ} 's positive, seemingly mixing $|\Psi_0\rangle$ and $-|\Psi_0\rangle$. Without knowing the ground state one does not know how to filter out the components with negative sign. One should also note the set of all possible Slater determinants is overcomplete and the members are not necessarily orthogonal; that is, we have

$$\langle\phi'|\phi\rangle \neq \delta_{\phi\phi'}, \quad \sum_{\phi} |\phi\rangle\langle\phi| \neq 1. \tag{2.32}$$

The initial state $|\Psi_T\rangle$ is usually chosen to be a single Slater determinant, defined by some matrix B_T , so we need to consider how to execute $U(\tau + \Delta\tau)|\phi\rangle$. The remarkable thing is that after using the Trotter approximation [23] to approximate $U(\tau + \Delta\tau)$ for small $\Delta\tau$ and using the discrete Hubbard-Stratonovich transformation [24] to transform the exponential of the potential energy, this imaginary-time evolution can be expressed as

$$\sum_{x=\pm 1} p(x)B(x)|\phi\rangle, \tag{2.33}$$

where $p(x) = \frac{1}{2}$ and $B(x)$ is the product of exponentials whose arguments are each quadratic forms of creation and destruction operators [5–7]. By Thouless' Theorem [25], the latter means the result of $B(x)|\phi\rangle$ is simply another single Slater determinant. What is happening is the Trotter approximation and Hubbard-Stratonovich transformation converts the interacting problem over a short imaginary time into a non-interacting one in a stochastic external field. A single Slater determinant is a non-interacting state. Each step of the iteration is thus propagating a non-interacting state by an effective non-interacting Hamiltonian and hence another non-interacting state evolves. If B' is the matrix describing this new Slater determinant and M is the matrix defining the quadratic form, then one can show that

$$B' = e^{-\Delta\tau M} B. \tag{2.34}$$

But there are two values of x ! A Monte Carlo method is used to sample one from $p(x)$; hence, only one Slater determinant is generated from any other one. Overall the strategy is to begin the simulation by replicating $|\Psi_T\rangle$ many times. For each, sample an independent value of x , say \bar{x} , from $p(x)$ and propagate that Slater determinant as $B(\bar{x})|\phi\rangle$. For one starting state, this is depicted in Fig. 3. Each starting state, a random walker, moves along a path in the space of all Slater determinants. By summing over the evolution of many starts, the various walkers sample many of the possible states that constitute the ground state, and after a sufficient number of iterations, the sum of the current Slater determinants will represent one sampling of the ground state wavefunction $|\Psi_0\rangle$. The iteration is continued until a sufficiently large number of statistically independent samples are accumulated so the error estimate for the measured quantities is acceptable.

Sampling efficiently, reducing the statistical error, and controlling the sign problem requires augmenting this strategy. Issues of efficiency and variance reduction are discussed in detail in the original papers and cannot be expressed as succinctly as how the sign problem is controlled. The sign problem is controlled by selecting a state $|\Psi_C\rangle$ that is a good approximation to the ground state and throwing away any random walker that does not satisfy $\langle\Psi_C|\phi\rangle > 0$. This is the constrained-path condition. Typically, one takes $|\Psi_C\rangle = |\Psi_T\rangle$. We also remark that one consequence of the variance reduction procedures is the assignment of a weight w_ϕ to each random walker $|\phi\rangle$ in the sample. The constrained-path condition amounts to setting the weights of violating walkers to zero.

The overcompleteness of the basis, Eq. (2.32), has some novel consequences for the interpretation of the constraint. In general, any $|\phi\rangle$ can be written as a linear combination

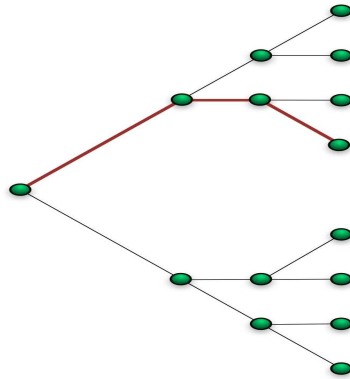


Figure 3: Schematic representation of a possible path in space of Slater determinants from one starting determinant relative to other possible paths. The space is continuous. At each Monte Carlo decisions there are two branches. The regularity depicted is for convenience.

of many other $|\phi\rangle$'s in the basis. The overcompleteness means that even if this number is infinity, the basis need not be exhausted. Further, because the thrown-away state overlaps the kept states, not all information carried by the terminated walker is lost. In short, the nodal surface defined by $\langle\Psi_T|\phi\rangle$ is not sharp and the solution does not strongly inherit its features. This situation contrasts that of the lattice fixed-node method.

The consequence of the constraint on the accuracy of measured quantities has been studied extensively by comparing predictions of the constrained-path method to those obtained by the Lanczos, density-matrix renormalization group, auxiliary-field, and lattice fixed-node methods. In general, the error of the constrained-path method is more controllable than that of the auxiliary-field method as the system size is increased. This is a consequence of the elimination of the sign problem. Its accuracy typically, but modestly, exceeds the fixed-node method [20, 26, 27]. Its results also display good insensitivity to the choice of $|\Psi_T\rangle$. Importantly, the method easily generates estimates of a variety of many-body correlations.

In computing estimates of a physical observable, the so called mixed estimator is used to obtaining the sample estimate of some observable X ,

$$\langle X \rangle = \sum_i w_i \frac{\langle\Psi_T|X|\phi_i\rangle}{\langle\Psi_T|\phi_i\rangle} / \sum_i w_i. \tag{2.35}$$

It is interesting to note that for the lattice fixed-node method this estimator provides a variational upper bound for the the ground state energy [27]. This is not true for the constrained-path method [7]. In general, the mixed estimate is not an upper bound for most observables.

The basic quantity computed is $\langle c_i^\dagger c_j \rangle$. If B_T is the matrix defining $|\Psi_T\rangle$ and B the

one defining $|\phi\rangle$, then

$$G_{ij} = \frac{\langle \Psi_T | c_j^\dagger c_i | \phi \rangle}{\langle \Psi_T | \phi \rangle} = \left[B (B_T^T B)^{-1} B_T^T \right]_{ji}, \quad (2.36)$$

which is readily computable during the simulation. The importance of this measurable is permitting the exploitation of the Trotter approximation and Hubbard-Stratonovich transformation's replacing the short-time imaginary-time propagation of any Slater determinant with the original interacting Hamiltonian by a propagation by a non-interacting Hamiltonian in a stochastic external field. The effective Hamiltonian being non-interacting means Wick's Theorem can be used to express averages such as $\langle c_i^\dagger c_j c_k^\dagger c_k \rangle$ by sums of products of the basic measurement

$$\begin{aligned} \langle c_i^\dagger c_j c_k^\dagger c_l \rangle &= \langle c_i^\dagger c_j \rangle \langle c_k^\dagger c_l \rangle + \langle c_i^\dagger c_l \rangle \langle c_j c_k^\dagger \rangle \\ &= \langle c_i^\dagger c_j \rangle \langle c_k^\dagger c_l \rangle + \langle c_i^\dagger c_l \rangle \left(\delta_{jk} - \langle c_k^\dagger c_j \rangle \right) \\ &= G_{ji} G_{lk} + G_{li} (\delta_{kj} - G_{jk}). \end{aligned} \quad (2.37)$$

As a closing note, we comment that the restriction of $|\Psi_T\rangle$ to a single Slater determinant is unnecessary. The computation cost will be proportional to the number used. While the results tend to be satisfyingly insensitive to the choice of this state, it is true that when a single Slater determinant is used, the best results are obtained when this choice represents a closed-shell solution to the non-interacting problem; that is, the number of electrons in both spin channels are a non-degenerate solution of the non-interacting problem. We also comment that while the Hartee-Fock solution of the interacting problem is a single Slater determinant using it does not necessarily improve the results over those obtained with the non-interacting solution. For open shell fillings, it is best if multiple Slater determinants are used.

3 Basic models

Explaining superconductivity, magnetism, and other electronic properties of real materials is challenging. To meet this challenge, many theoretical models have been proposed whose electronic structures are simpler than those produced by *ab initio* methods but have features hopefully representing the essential physical processes at least qualitatively. Among these models, the simplest and most studied model is the Hubbard model [28, 29]. This is a one-band model with one lattice site per unit cell and one non-degenerate orbital per lattice site. Nevertheless, the physics of this model is rich and includes antiferromagnetism, a Hubbard-Mott metal-insulator transition, and phase separation. In contrast to this simple one-band model, several multi-band models have also been actively studied and are believed to explain the often surprising states of matter observed experimentally. In this review, we will discuss the three-band Hubbard model [30], periodic Anderson model,

and Falicov-Kimball [31] model. In the three-band model, the multiband character arises from the model having three lattice sites per unit cell. A single non-degenerate orbital occupies each site. In the periodic Anderson model, there is one lattice site per unit cell. The multiband character arises from that site being occupied by a two-orbital atom. The Falicov-Kimball model also has a double non-degenerate orbital atom on each site of a one site unit cell, but in contrast to the periodic Anderson model, the electrons are usually spinless.

The original purpose of each Hamiltonian was the modelling of distinctly different physics. The three-band Hubbard model, for example, was proposed to explain the physics of the high- T_c superconductors so pairing correlations have been the main quantities computed. Often physics other than that initially intended is also modelled. For example, the periodic Anderson model, which was developed to study heavy fermion and Kondo physics, has so far proven to exhibit these phenomena limitedly, but instead has displayed a strong presence of ferromagnetism with a variety of mechanisms producing itinerant ferromagnetism. Similarly, the Falicov-Kimball model, developed for metal-insulator transitions and mixed valent behavior, has been found to possess a novel electronic ferroelectric state co-existing with a coherent chiral state of ordered atomic currents. Indeed, many of these surprises would have remained hidden or controversial without numerical analysis of the properties of these models.

3.1 Three-band hubbard model

The three-band Hubbard model [30] was proposed as a minimal model to investigate the high- T_c superconductivity in the cuprates. This definition is restricted to a two-dimensional plane describing the CuO_2 layer distinctively common in these materials where the valence electrons occupy $3d_{x^2-y^2}$, $2p_x$ and $2p_y$ orbitals.

The Hamiltonian is

$$\begin{aligned}
 H = & \sum_{\langle j,k \rangle \sigma} t_{pp}^{jk} (p_{j\sigma}^\dagger p_{k\sigma} + p_{k\sigma}^\dagger p_{j\sigma}) + \varepsilon_p \sum_{j\sigma} n_{j\sigma}^p + U_p \sum_j n_{j\uparrow}^p n_{j\downarrow}^p \\
 & + \sum_{\langle i,j \rangle \sigma} t_{pd}^{ij} (d_{i\sigma}^\dagger p_{j\sigma} + p_{j\sigma}^\dagger d_{i\sigma}) + \varepsilon_d \sum_{i\sigma} n_{i\sigma}^d + U_d \sum_i n_{i\uparrow}^d n_{i\downarrow}^d + V_{pd} \sum_{\langle i,j \rangle} n_i^d n_j^p, \quad (3.1)
 \end{aligned}$$

where the operator $d_{i\sigma}^\dagger$ creates a *hole* with spin σ in a Cu $3d_{x^2-y^2}$ -orbital and $p_{j\sigma}^\dagger$ creates a *hole* with spin σ in an O $2p_x$ or $2p_y$ -orbital. U_d and U_p are the Coulomb repulsions at the Cu and O sites, ε_d and ε_p are the corresponding orbital energies, and V_{pd} is the nearest neighbor Coulomb repulsion. As written, the model has a Cu-O hybridization $t_{pd}^{ij} = \pm t_{pd}$ with the minus sign occurring for $j = i + \hat{x}/2$ and $j = i - \hat{y}/2$ and also an O-O hybridization $t_{pp}^{jk} = \pm t_{pp}$ with the minus sign occurring for $k = j - \hat{x}/2 - \hat{y}/2$ and $k = j + \hat{x}/2 + \hat{y}/2$. These phase conventions are illustrated in Fig. 4. For the non-interacting model ($U_p = V_{pd} = 0$)

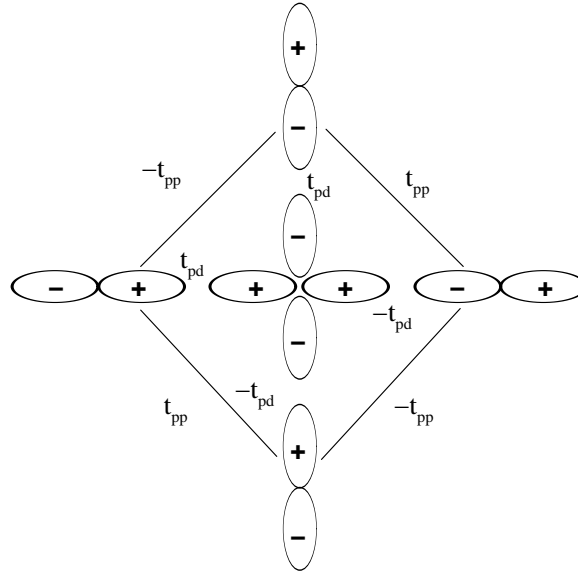


Figure 4: Phase convention for the hopping matrix elements. The copper $d_{x^2-y^2}$ orbital is surrounded by the oxygen p_x and p_y orbitals. The hopping matrix elements are shown with their corresponding phase.

with $t_{pp} = 0$, a typical band structure is shown in Fig. 5. The bands are given by

$$\begin{aligned}
 E^\pm(k_x, k_y) &= \frac{1}{2} \left[\varepsilon_d + \varepsilon_p \pm \sqrt{(\varepsilon_d - \varepsilon_p)^2 + 16t_{pd}^2 \left(\sin^2 \frac{k_x}{2} + \sin^2 \frac{k_y}{2} \right)} \right], \\
 E^m(k_x, k_y) &= \varepsilon_p.
 \end{aligned} \tag{3.2}$$

To investigate possible superconductivity mechanisms, the extended s -wave and the $d_{x^2-y^2}$ -wave pairing correlations as functions of distance are studied. The pairing correlation functions have the following form

$$P_\alpha(R) = \langle \Delta_\alpha^\dagger(R) \Delta_\alpha(0) \rangle, \tag{3.3}$$

where

$$\begin{aligned}
 \Delta_\alpha(R) &= \sum_{\delta} f_\alpha(\delta) [(d_{R\uparrow} d_{R+\delta\downarrow} - d_{R\downarrow} d_{R+\delta\uparrow}) \\
 &\quad + (p_{R\uparrow}^x p_{R+\delta\downarrow}^x - p_{R\downarrow}^x p_{R+\delta\uparrow}^x) + (p_{R\uparrow}^y p_{R+\delta\downarrow}^y - p_{R\downarrow}^y p_{R+\delta\uparrow}^y)],
 \end{aligned} \tag{3.4}$$

with $\delta = \pm\hat{x}, \pm\hat{y}$ in a square lattice. The pairing symmetry is defined through the function $f_\alpha(\delta)$. For the extended s -wave pairing $f_{s^*}(\delta) = 1$ for all δ and for $d_{x^2-y^2}$ -wave pairing, $f_d(\delta) = 1$ for $\delta = \pm\hat{x}$ and $f_d(\delta) = -1$ for $\delta = \pm\hat{y}$.

The magnitude of $P_\alpha(R)$ is dominated by a large peak when $|R|$ is less than a few nearest neighbor distances. Over these distances, P_α measures local correlations among spin

and charge, has little information about long-range pairing correlations, and may give a “false positive” indication of enhanced pairing. Because of this, one usually reports neither the $q = 0$ spatial Fourier transformation nor the partial sums like $S_\alpha(L) = \sum_{|R| \leq L} P_\alpha(R)$ but instead reports partial averages [32,33] like $V_\alpha^{ave}(R > L) = \frac{1}{N'} \sum_{|R| > L} V_\alpha(R)$ where L is about two lattice spacings, and N' is the number of distances larger than L . In fact, we will mainly report such averages for the “vertex contribution” to the correlation functions defined as [34]

$$V_\alpha(R) = P_\alpha(R) - \bar{P}_\alpha(R) , \tag{3.5}$$

where $\bar{P}_\alpha(R)$ is the contribution of dressed non-interacting propagator: for each term in $P_\alpha(R)$ of the form $\langle c_\uparrow^\dagger c_\uparrow c_\downarrow^\dagger c_\downarrow \rangle$, $\bar{P}_\alpha(R)$ has a term like $\langle c_\uparrow^\dagger c_\uparrow \rangle \langle c_\downarrow^\dagger c_\downarrow \rangle$.

3.2 Periodic Anderson model

The periodic Anderson model (PAM) is one of the principal models for the low temperature properties of heavy fermion and dense Kondo solids. These materials are typically rare-earth and actinide metallic compounds that exhibit several different kinds of ground states: antiferromagnetic, superconducting, paramagnetic, or semiconducting [35]. On the other hand, the periodic Anderson model has been found to be a likely candidate as the minimal lattice model for itinerant ferromagnetism, phenomena that is rare in these materials [36–40]. A very simple extension of this model makes it a possible description for many transition metals [41, 42].

The Hamiltonian for a generalized periodic Anderson model is

$$\begin{aligned}
 H = & -t_d \sum_{i,j,\sigma} (d_{i\sigma}^\dagger d_{j\sigma} + d_{j\sigma}^\dagger d_{i\sigma}) - t_f \sum_{i,j,\sigma} (f_{i\sigma}^\dagger f_{j\sigma} + f_{j\sigma}^\dagger f_{i\sigma}) + \epsilon_f \sum_{i,\sigma} n_{i\sigma}^f \\
 & + V \sum_{i,\sigma} (d_{i\sigma}^\dagger f_{i\sigma} + f_{i\sigma}^\dagger d_{i\sigma}) + U \sum_i n_{i\uparrow}^f n_{i\downarrow}^f ,
 \end{aligned} \tag{3.6}$$

where $d_{i\sigma}^\dagger$ and $d_{i\sigma}$ creates and annihilates a conduction electron with the spin σ at the lattice site i , and $f_{i\sigma}^\dagger$ and $f_{i\sigma}$ creates and annihilates a f -electron. $n_{i\sigma}^f = f_{i\sigma}^\dagger f_{i\sigma}$ is the electron number operator. Here t_d and t_f are the hopping matrix elements for conduction and localized electrons and the t_d and t_f hoppings are only to nearest-neighbor sites. ϵ_f is the energy of the localized f -orbital, U is the on-site Coulomb repulsion of the f electrons. The hopping amplitude V hybridizes different orbitals on the same site. If the designation d and f were taken literally, the on-site hybridization would be unphysical because such orbitals have opposite spatial parity. The intent is merely to model the likely hybridization of two different orbitals in the simplest way. If the parity of the orbitals matters, the model is easily adaptable. When $t_f = 0$, the Hamiltonian is the standard PAM.

When $U = 0$, there are two bands that in two dimensions are given by

$$E^\pm(k_x, k_y) = \frac{1}{2} \left[\epsilon_d + \epsilon_f \pm \sqrt{(\epsilon_d - \epsilon_f)^2 + 4V^2} \right] , \tag{3.7}$$

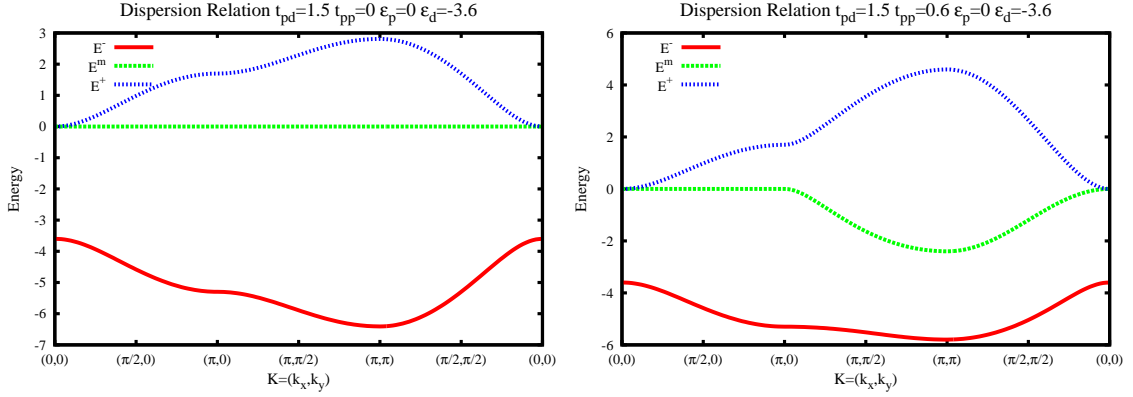


Figure 5: Dispersion of the three-band Hubbard model (a) for the case of zero t_{pp} and (b) for the case of Negro t_{pp}

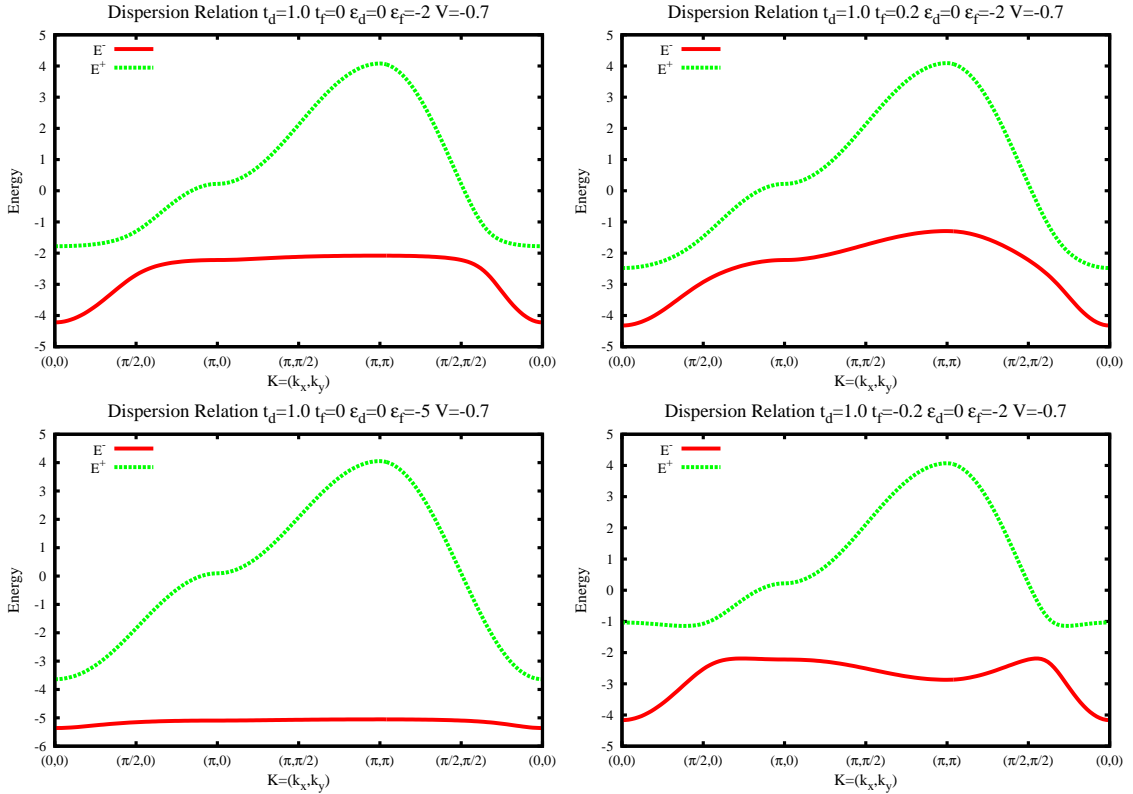


Figure 6: Dispersion of the periodic Anderson model (a) for the case of zero t_f , (b) for the case of positive t_f (c) for the case of zero t_f with a large band gap, (d) for the case of negative t_f

where

$$\epsilon_d = -2t_d(\cos k_x + \cos k_y), \quad \epsilon_f = \epsilon_f - 2t_f(\cos k_x + \cos k_y). \quad (3.8)$$

Fig. 6 shows typical two-dimensional band structures. When $t_f = 0$, a band gap always

exists. When $t_f \neq 0$, the qualitative features of the band structure can change. Principally, when $|t_f|$ becomes sufficiently large, the gap closes.

The magnetic properties of the periodic Anderson model are investigated through the computation of two quantities. One is the energy as a function of the total spin $E(S)$. If the total number N_T of electrons satisfies $N \leq N_T \leq 2N$, where N is the number of lattice sites, have been studied, and if $N_\uparrow \geq N_\downarrow$, the difference $\frac{1}{2}(N_\uparrow - N_\downarrow)$ is the z-component of the total spin S^z . Because the total spin S and S^z commute with the Hamiltonian H , we can set $S = S^z$ and compute the ground state energy of H as a function of S . If $E(S)$ is a minimum for $0 < S < N$, the ground state is a partially saturated ferromagnetically. If $E(S)$ is a minimum for $S = N$, the saturation is full. By plotting $E(S)$ versus S , we can tell if the ground state is ferromagnetic.

If the minimum occurs for $S = 0$, the ground state is unpolarized (paramagnetic or antiferromagnetic). Further information about the spin structure of the ground state is obtained by computing the Fourier transform of the spin-spin correlation function

$$S(k) = \frac{1}{N} \sum_{i,j} \langle S_i^z S_j^z \rangle e^{ik \cdot (x_i - x_j)}, \quad (3.9)$$

where $S_i^z = \frac{1}{2}(n_{i\uparrow}^f - n_{i\downarrow}^f)$, x_i its the lattice position, and $\langle S_i^z S_j^z \rangle$ is the ground state expectation value of the product of the two spins at sites i and j . Since most of the magnetism of the system comes from the polarization of the f -electrons, this usually is the most relevant correlation functions. (An analogous one can be defined for the d -electrons.) By analyzing the correlation spectrum, one can distinguish which type of magnetic ordering exists in the system. For example, in two dimensions, if a large peak exists at the wavevector (π, π) , antiferromagnetic ordering exists; if a large peak exists at the wavevector $(0, \pi)$ and $(\pi, 0)$, a resonating spin density wave exists. If these peaks extrapolate to non-zero values as the lattice size is increased toward infinity (the thermodynamic limit), then a state of long-range order exists.

3.3 Falicov-Kimball model

Introduced forty years ago to describe the semiconductor-metal transition in SmB_6 and related materials, the Falicov-Kimball model [31], while appearing very simple, exhibits an array of rich and interesting properties. Under certain restrictions, many of its properties have been determined analytically. For example, for the original version of the model, in any dimension greater than 1, and for any value of its repulsive interaction between the electrons, its equilibrium states display long-range charge ordering of the chessboard type provided the temperature is low enough [43]. Away from 1/2-filling, i.e., when the total electron densities differs from 1, the electrons segregate at zero temperature when the repulsion is large enough. Not all properties have been as accessible analytically. Recently, a proposal that the model exhibits a novel electronic ferroelectric state model was made [44,45], and more recently this was successfully demonstrated through a combination of analytic and numerical work [8–10]. In this review, we will summarize results for the

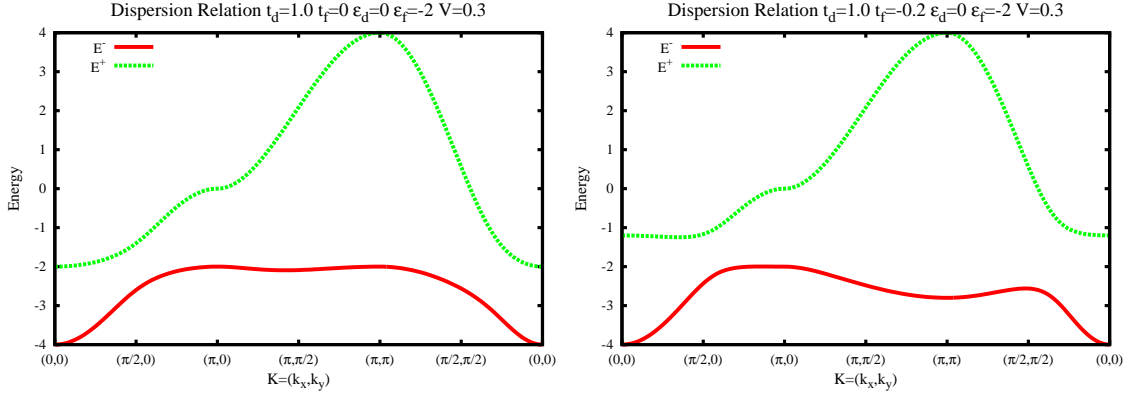


Figure 7: Dispersion of the Falicov Kimball model (a) for the case of zero t_f , (b) for the case of nonzero t_f

charge structure simulations and will present results for the electronic ferroelectric state, plus the other interesting states, such as orbital ordering, exhibited by this model.

The generalized Falicov-Kimball Hamiltonian we consider is

$$\begin{aligned}
 H = & -t_d \sum_{\langle i,j \rangle} (d_i^\dagger d_j + d_j^\dagger d_i) + \epsilon_d \sum_i n_i^d - t_f \sum_{\langle i,j \rangle} (f_i^\dagger f_j + f_j^\dagger f_i) + \epsilon_f \sum_i n_i^f \\
 & + V \sum_{i,\nu=\hat{x},\hat{y}} (d_i^\dagger f_{i+\nu} + f_{i+\nu}^\dagger d_i - f_i^\dagger d_{i+\nu} - d_{i+\nu}^\dagger f_i) + U \sum_i n_i^d n_i^f, \quad (3.10)
 \end{aligned}$$

where ϵ_d and ϵ_f are the d and f orbital energies, t_d and t_f are the hopping integrals between neighboring d and f -orbitals, V is the off-site hybridization between the orbital, and U is the inter-orbital Coulomb interaction. The off-site hybridization assumes the d and f -orbitals have opposite parity under spatial inversion ($t_d = -t_f$). For the non-interacting problem the energy bands are given by

$$E^\pm(k_x, k_y) = \frac{1}{2} \left[(\epsilon_d + \epsilon_f)^2 \pm \sqrt{(\epsilon_d - \epsilon_f)^2 + 16V^2 (\sin k_x + \sin k_y)^2} \right], \quad (3.11)$$

where

$$\epsilon_d = \epsilon_d - 2t_d(\cos k_x + \cos k_y), \quad \epsilon_f = \epsilon_f - 2t_f(\cos k_x + \cos k_y). \quad (3.12)$$

Figure 7 illustrates typical two-dimensional band structures. To some extent, this generalized Falicov-Kimball model is close to being a spinless version of the periodic Anderson model. The key difference is the form of the band hybridization term necessitated by the assumption of the different parity of the orbitals. The original version of the model had $t_f = V = 0$ and the relative parity of the orbitals was unspecified. Correlations functions of the pseudo-spins are used to identify orbital orderings. These components are defined by

$$\tau_i^x = \frac{1}{2}(d_i^\dagger f_i + f_i^\dagger d_i), \quad \tau_i^y = \frac{i}{2}(d_i^\dagger f_i - f_i^\dagger d_i), \quad \tau_i^z = \frac{1}{2}(f_i^\dagger f_i - d_i^\dagger d_i). \quad (3.13)$$

They are called pseudo-spin because they obey the same commutation relations as the physical spin-1/2 components of angular momentum.

$$[\tau_i^x, \tau_j^y] = \tau_i^z \delta_{ij}, \quad [\tau_i^y, \tau_j^z] = \tau_i^x \delta_{ij}, \quad [\tau_i^z, \tau_j^x] = \tau_i^y \delta_{ij}. \quad (3.14)$$

The pseudospin-pseudospin correlation functions are defined in analogy to the spin-spin correlation functions

$$S^\alpha(k) = \frac{1}{N} \sum_{i,j} \langle \tau_i^\alpha \tau_j^\alpha \rangle e^{ik \cdot (x_i - x_j)}, \quad (3.15)$$

where $\alpha = x, y$, or z . (These are pseudo-directions.) If $S^z(k)$ peaks at a non-zero value of k , this is an indication of a modulation of the relative density of d and f -orbitals, that is, an ordering of atomic orbitals. Peaks in $S^x(k)$ and $S^y(k)$ are indicators of more novel types of ordering. As τ_i^x relates to an on-site hybridization, something that is symmetry forbidden, a peak in $S^x(k)$ at $k = 0$ would indicate the development of a spontaneous broken time-reversal symmetry. A peak in $S^y(k)$ signifies the development of a chiral state, an ordering of atomic currents. As we will discuss later, when $t_d = -t_f$, such states do develop and are accompanied by the appearance of a ferroelectric state.

4 Numerical results

4.1 Three-band Hubbard model

The three-band Hubbard model (3.1) is obviously more complicated than the one-band model. It has more degrees of freedom and a much larger parameter space. Studying it numerically thus requires more resources to perform systematic studies so these studies have been limited to smaller lattices and less comprehensive ranges of parameters. Nevertheless, there still have been many attempts to use numerical methods to investigate its magnetic and superconducting properties. For example, Scalettar *et al.* [32, 46] and Dopf *et al.* [33, 47–49] did QMC simulations at finite temperatures. However, the infamous sign problem, which is even more severe for the three-band model than for the single-band model, further limited these studies to relatively high temperatures. Similar to the single-band model, they found an anti-ferromagnetic state at 1/2-filling which is strongly suppressed upon doping. With regard to the existence of superconductivity, their results remain controversial: At finite temperatures, attractive interactions between pairs were found, but separate claims of extended s-wave [33, 47] and d-wave superconductivity [46] were made.

Avoiding the sign problem several groups did ED studies [50–53] of hole binding energies, and several other groups [54–59] performed zero-temperature QMC (including CPMC) computations calculations of superconducting pairing correlation functions. The ED studies unequivocally established that holes can bind, and the auxiliary-field projector QMC studies established the existence of an extended s-wave and $d_{x^2-y^2}$ -wave attractive pairing interaction [55–57], with one claim of no evidence of s-wave superconductivity [54].

The CPMC studies carried out by Guerrero and Gubernatis [58] and Huang *et al.* [59] confirmed the ED result that holes bind but found that increasing system size tended to decrease the long range part of the pairing correlations. In contrast to the ED work, the CPMC studies found hole binding in the absence of a Coulomb repulsion V_{pd} between charge on neighboring Cu and O sites in contrast to the ED studies which found that hole binding requires an unphysically large value of V_{pd} .

With this preview, we will now review the studies in more detail and focus on three issues: (i) the charge distribution (that is, where do the doped holes go?) (ii) the existence of antiferromagnetic long-range order at 1/2-filling and its disappearance upon hole doping away from half filling, and (iii) the existence of superconductivity.

With regard to the charge distribution, almost all results show that the holes mainly distribute themselves onto the O sites, even when the difference between the O and Cu orbital energies $\epsilon = \epsilon_p - \epsilon_d$ is relatively large. There are basically two regimes in the parameter space: the charge transfer regime, $U_d > \epsilon > W$ and $V_{pd} > 0$, and the mixed-valent regime, $U_d > W > \epsilon$, where W is the bandwidth for non-interacting case. In the charge transfer regime, V_{pd} is expected to induce charge transfer from the O to the Cu sites as it is increased. The transfer rate should also increase if ϵ is increased. On the other hand, in the mixed-valent regime, the transfer is holes from the Cu to the O sites. Here, ϵ is small and a strong on-site repulsive U_d , favoring charge transfer from the Cu sites, should dominate the smaller repulsive V_{pd} which opposes the movement of charge to the O sites. These trends were also observed in the finite-temperature QMC [47], the CPMC studies [59], and zero-temperature exact diagonalization [46] studies. An important conclusion is that in the physically relevant charge transfer region, hole binding energy is mainly gained from magnetic mechanisms, rather than from the so called electronic polarization mechanism suggested by early exact diagonalization studies at the limit $U_{Cu} = U_O = \infty$ [53].

The local magnetic moment and spin-spin correlation function are typically calculated to understand the magnetic properties of the model. Fig. 8 shows the magnetic moment on the Cu site as a function of V_{pd} and doping. These results were obtained from a CPMC simulation of a 6×6 lattice by Huang *et al.* [59]. For a given ϵ , increasing the hole doping increases the moment, while for a given doping, increasing ϵ also increases the moment. The effect of V_{pd} depends on the value of ϵ , showing the moment increase being strongly correlated with the charge on the Cu sites.

An important feature of the cuprates is the appearance of incommensurate peaks in neutron scattering measurements of the spin-spin correlation functions. Similar peaks are observed in the CPMC calculations of this function for the three-band model, and typical results are shown in Figs. 7 and 8 in the Ref. [59]. As shown, there are two principal peaks in the Fourier transform of the static Cu spin-spin correlation function: one is the displaced antiferromagnetic peak at $(\pi, \pi - \delta)$ and the other is the incommensurate peak at $(\pi - \delta', \pi - \delta')$. This latter peak was also observed in the numerical simulations of the single-band Hubbard model [60–62], and it qualitatively agrees with the experimental data for $(\text{La}_{1-x}\text{Sr}_x)_2\text{CuO}_4$ [63], where a minimum is observed at (π, π) along the diagonal

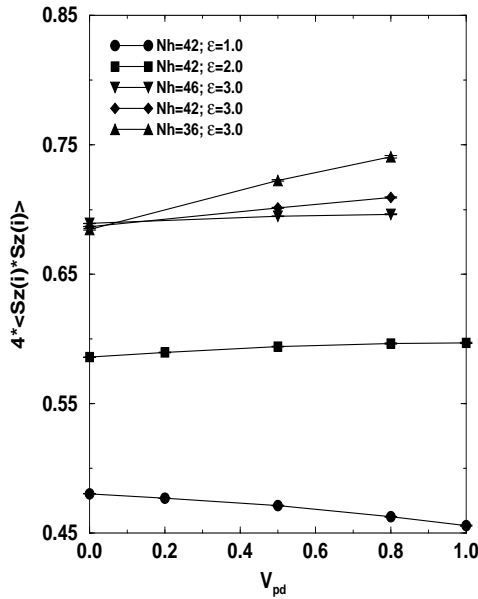


Figure 8: A typical magnetic moment on the Cu site as a function of V_{pd} and doping concentration [59].

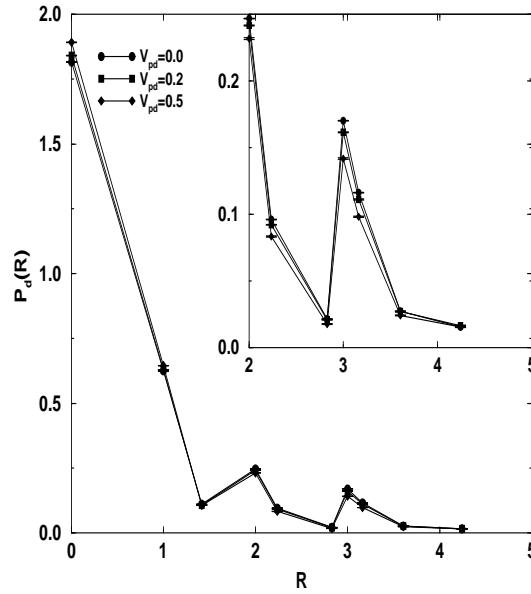


Figure 9: A typical d-wave pairing correlation function as a function of distance and V_{pd} [59].

direction.

The three-band model has an important additional parameter that the one-band model lacks, the hopping between oxygen sites t_{pp} . The value of this parameter strongly influences the incommensurate peak along the diagonal direction. Huang *et al.* [59] showed that even for a very small t_{pp} , a weak peak exists at $(\pi - \delta', \pi - \delta')$. On increasing t_{pp} , the spin-spin correlations are strongly suppressed near the antiferromagnetic wave vector (π, π) , and at the same time the amplitude of the incommensurate peak along the diagonal direction, or simply the tendency to form this peak, is enhanced. Studies of the magnetic structure factor also showed that antiferromagnetism at 1/2-filling is destroyed by hole doping, similar to the destruction seen in the single-band model. For 1/2-filling, increasing t_{pp} greatly suppresses antiferromagnetic order. These results suggest that t_{pd} , U_d , and ϵ are the most important parameters for the intrinsic physics of cuprates compounds.

Finally, we come to the most relevant question for studying the three-band model, Does it support an electronic mechanism for superconductivity? To answer this question, the long distance behavior of the pairing correlation function was studied. Shown in Fig. 9 is a typical *d*-wave pairing correlation function as a function of distance and V_{pd} . Here, we observe a large peak at short distances ($|R| < 2$). At these distances, increasing V_{pd} increases the magnitude of the correlations slightly. At larger distances ($|R| > 2$), the trend reverses. The dominance of the local peak means the $\mathbf{k} = 0$ Fourier transform of the pairing correlation function, that is, the integral of $P(R)$ with a large distance cut-off, exhibits behavior indicative only of short-range behavior and hides the more relevant long-

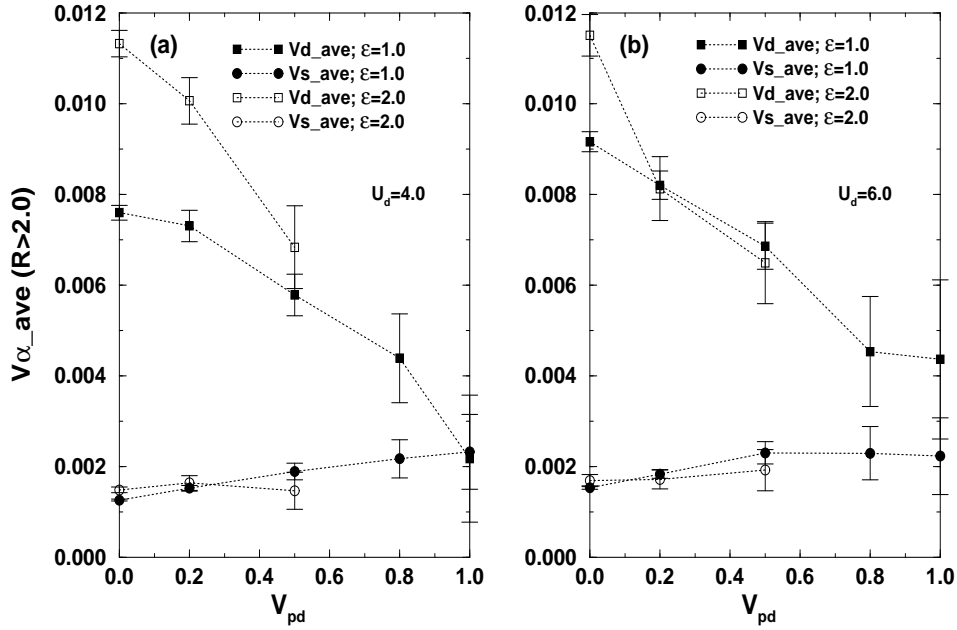


Figure 10: The long-range (average over $R > 2$) behavior of the $d_{x^2-y^2}$ -wave and extended s-wave pairing correlations [59].

range behavior. In Fig. 10 is the long-range behavior of the $d_{x^2-y^2}$ -wave and extended s-wave pairing correlation functions averaged over $R > 2$. As a function of distance, they both decay quickly. In the charge-transfer regime, increasing V_{pd} decreases the long-range part of both correlation functions, while in the mixed-valent regime, it increases the long-range part of the s-wave behavior but decreases that of the d-wave behavior. For all cases simulated, the long-range part of the d-wave contribution is consistently larger than the s-wave contribution. However, these correlations are rather weak, and their dependence on lattice size is similar to that found for the d-wave pairing correlation functions of the single-band model; namely, increasing the lattice size systematically suppresses the long-ranged parts of these correlations.

4.2 Periodic Anderson model

Early numerical works on the PAM dealt mainly with the symmetric case ($U = -\varepsilon_f/2$) of the standard Hamiltonian

$$\begin{aligned}
 H = & -t_d \sum_{i,j,\sigma} (d_{i\sigma}^\dagger d_{j\sigma} + d_{j\sigma}^\dagger d_{i\sigma}) \\
 & + V \sum_{i,\sigma} (d_{i\sigma}^\dagger f_{i\sigma} + f_{i\sigma}^\dagger d_{i\sigma}) + U \sum_i n_{i\uparrow}^f n_{i\downarrow}^f, \quad (4.1)
 \end{aligned}$$

at 1/2-filling (2 electrons per lattice site). For instance, Blankenbecler *et al.* [64], in particular, performed a QMC calculation on a finite chain up to 16 sites and observed short-ranged antiferromagnetic correlations. These results were confirmed by subsequent ED work [65–67]. Ueda *et al.*, in particular, studied the importance of RKKY and Kondo interactions to the stability of the ground state. For the 2D case, Zhang *et al.* [68] used a QMC method to study spin-spin correlation functions and susceptibilities on 4×4 and 6×6 square lattices. Later, Callaway *et al.* [69–72] performed ED studies and confirmed the work of Zhang *et al.* All the numerical results were consistent with analytic results [73–75].

An important issue for the PAM is the nature of its charge transfer gap. The system can be metal or insulator depending on the value of the Coulomb interaction U_f , f -orbital energy ε_f , and the hybridization V between the d and f -bands. Using ED, Nishino *et al.* [76] studied the dependence of the spin excitation $\Delta(s)$ and charge excitation $\Delta(c)$ gaps for 1/2-filled chains up to 8 sites as a function of the Coulomb coupling U_f . They observed that the ratio of the gaps, $R = \Delta(c)/\Delta(s)$, increases monotonically from unity when $U_f = 0$ and diverges in the strong-coupling limit. In particular, $\Delta(s)$ decreases exponentially as U_f is increased but $\Delta(c)$ at the same time decreases much more slowly. This behavior was later confirmed by Tian's rigorous result [77,78].

When the f -band is dispersive, Guerrero *et al.*'s DMRG work [79,80] gave some additional insight. For $U_f = 0$, a small dispersion in the f -band can close the hybridization and hence the charge transfer gap. In contrast, when U_f is large, the dispersion has little effect on the charge transfer gap. This suggests that for a given dispersion, a metal-insulator transition may occur at a critical value of the Coulomb repulsion U_f^c . An analytic calculation shows that this transition in fact occurs at $U_f = 0$. In contrast to this behavior for the charge transfer gap, the spin gap is strongly suppressed as U_f is increased. This suppression is associated with the enhancement of antiferromagnetic correlations, with the spin gap closing when U_f is increased enough so an antiferromagnetic state develops.

Before investigating the magnetic properties of PAM for fillings far away from 1/2-filling, the effect of doping away from 1/2 filling should be mentioned. Bonča *et al.* [81] found the non-monotonic effect of doping, which means doping does not always enhance or reduce the magnetism. The reason why lies in the features of the band structure, segmented features and Fermi surface nesting for some given parameters.

Mapping the phase diagram of the system is always the most interesting challenge. Considerable numerical and analytic work has been poured into this. Since the lattice sizes typically are less than what is needed to extrapolate to the thermodynamic limit, only the broad features as opposed to precise boundaries, are obtained. The interesting parameter region was found from 1/4 to 1/2-filling with different hybridizations V , f -orbital energies ε_f , and Coulomb interactions U_f .

For perspective, we first consider the phase diagram obtained by Moller and Wolffe [82] by using the slave-boson theory mean-field of Kotliar and Ruckenstein [83]. They studied the ground state of the symmetric, finite U , periodic Anderson model and found at 1/2-filling a charge gap for all $U > 0$ and a transition from a paramagnetic to an antiferromagnetically ordered (AF) state at a critical value of U for given value of V .

The AF state was the one lowest in energy within a manifold of spiral magnetic states. Results for the energy, hybridization matrix element, and local moment compared well with quantum Monte Carlo results for finite systems. Lowering the electron density induces a smooth crossover from AF to ferromagnetic (FM) order via a spiral phase. Just above 1/4-filling, they found a first order transition from FM to AF order. The insulating state at 1/4-filling was well described by an AF Heisenberg model.

In 1996 Guerrero *et al.* [84] used the DMRG method to obtain the magnetic phase diagram of the 1D PAM as a function of band filling. For strong coupling, the 1/4-filled system (one electron per site) has an $S = 0$ ground state with strong antiferromagnetic correlations. As electron filling increases, they found first a ferromagnetic phase, as also reported by Moller and Wolffe [82], and then a singlet ($S = 0$) phase. Within this phase, they reported Ruderman-Kittel-Kasuya-Yosida (RKKY) oscillations in the spatial dependence of spin-spin correlation functions.

Using the constrained-path Monte Carlo method, Batista *et al.* [37] and Wang *et al.* [85] studied the magnetic properties of the two-dimensional periodic Anderson model for electron fillings from 1/4 to 1/2. For 1/4-filling, they found that the system can be a Mott or a charge-transfer insulator, depending on the relative values of the Coulomb interaction and the charge-transfer gap between the two noninteracting bands. The insulator may be a paramagnet or antiferromagnet. Upon electron doping away from 1/4-filling, they observed a partially saturated ferromagnetic phase for a variety of parameter combinations. Provided the system was a charge-transfer insulator, the ferromagnetism was induced by the RKKY interaction. The regions of ferromagnetism spanned a much smaller doping range than suggested by the above slave boson [82] and dynamical mean-field theory (DMFT) calculations [86, 87], but they were consistent with those obtained by Guerrero *et al.* for the one-dimensional periodic Anderson model. For fillings between 3/8 and 1/2, Bonca and Gubernatis [81] predicted a PM region, whereas mean-field theory predicts ferromagnetic states in part of that region. In fact, at a filling of 3/8, where DMFT calculations predict ferromagnetism, they found a spin-density-wave state with a wave vector equal to $(\pi, 0)$ or $(0, \pi)$.

The ED method was also applied to the PAM to study its magnetism. Wang *et al.* [85] carried out calculations for a 6 and 8 site chain. For the 6-site chain, their simulations ranged from 1/4 to 1/2-filling with different f -band dispersions but with typical values of ε_f and V . For the 8-site chain, they conducted their simulations only for the number of electrons $N_e = 6, 8$, and 10. The energy $E(S)$ versus magnetization S curves and wavevector dependent spin-spin correlation functions were computed to determine which magnetic state is stable in the ground state. $E(S)$ versus S curves for the 6-site chain are shown in Fig. 11 and the spin-spin correlations are shown in Fig. 12. From the figures the magnetic regions are observed emerging in the paramagnetic (nonmagnetic) regime. Antiferromagnetism is observed around 1/2 and 1/4-filling for appropriate parameters. Ferromagnetic states are stable for fillings between 1/4 and 3/8, which qualitatively agrees with above DMRG and QMC works [36, 38].

The existence of antiferromagnetism at 1/4 and 1/2-fillings is suggested by the follow-

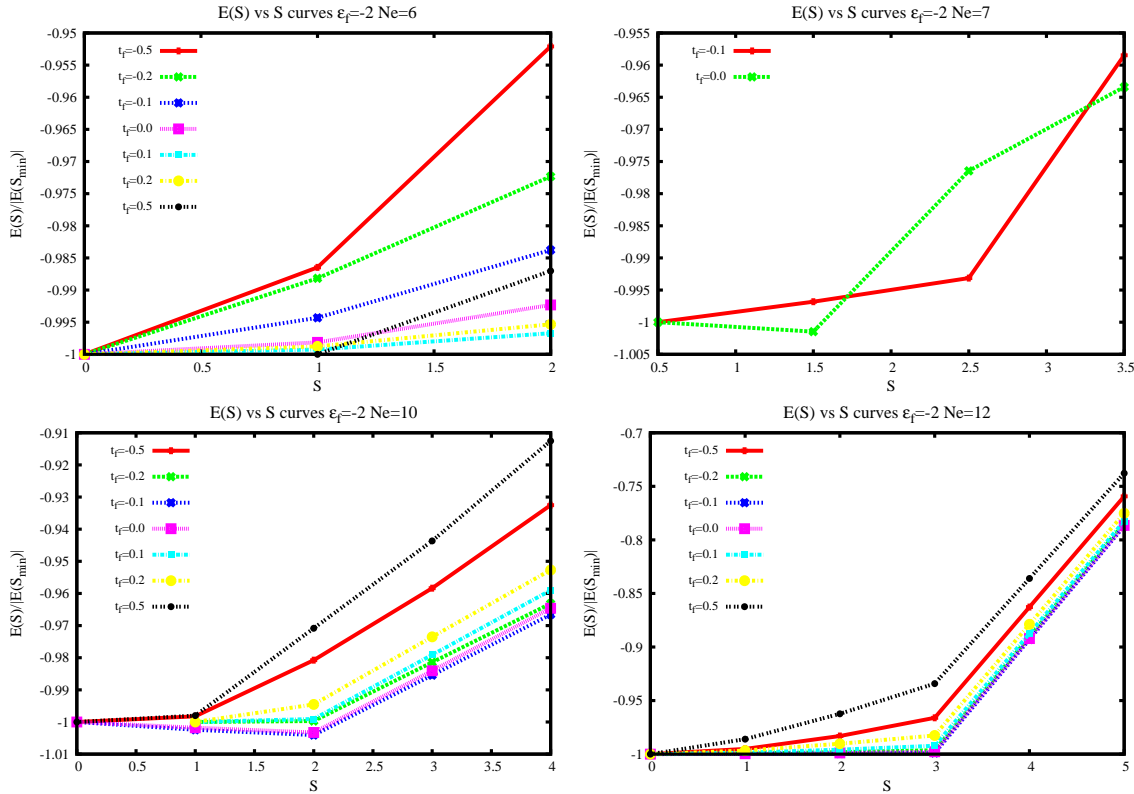


Figure 11: $E(S)$ versus S curves for 1/4 to 1/2 filling and $\varepsilon_f = -2$ with $V = -0.5$ on a 6-site chain [85].

ing argument. For 1/4-filling, a very negative f -electron orbital energy places one electron per f -orbital, and the resulting system behaves like a one-band 1/2-filled Hubbard model which is antiferromagnetic. This is illustrated in Fig. 12. For 1/2-filling, with relatively small values of the f -electron orbital energy and V , but a large value of U_f , one electron per f -orbital, (and d -orbital) is induced, and again the system is like the Hubbard model, but now weakly coupled to a non-interacting environment of d -electrons. This is illustrated in the last plot of Fig. 12.

The mechanism for ferromagnetism between 1/4 and 3/8-fillings is less obvious [36–40, 81, 86–89]. The work of Batista *et al.* [38, 39, 89] established that more than one exists, with none consistent with the traditional one, extracted from mean-field theories, of a competition between RKKY and Kondo interactions. For example, in the mixed valent state, Batista *et al.* attributed the appearance of ferromagnetism to a segmented band mechanism (Fig. 13). In this mechanism, the effect of the Coulomb interaction is the promotion of electrons near the Fermi energy into unoccupied f -states associated with the lower bands. These electrons align ferromagnetically so the spatial part of their wavefunction is antisymmetric and supports the reduction of the Coulomb interaction by allowing spatial separation of the electron. The basic competition is between two energy

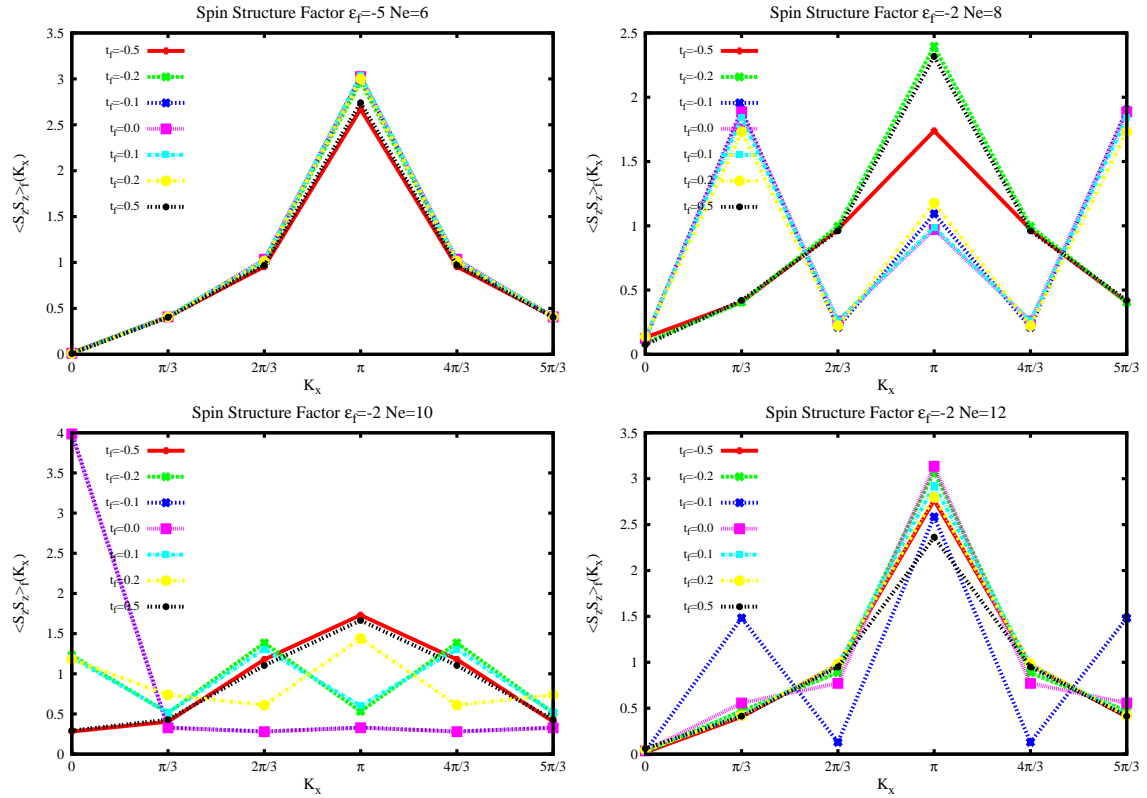


Figure 12: Spin structure factor curves for 1/4 to 1/2 filling with $V = -0.5$ on a 6-site chain [85].

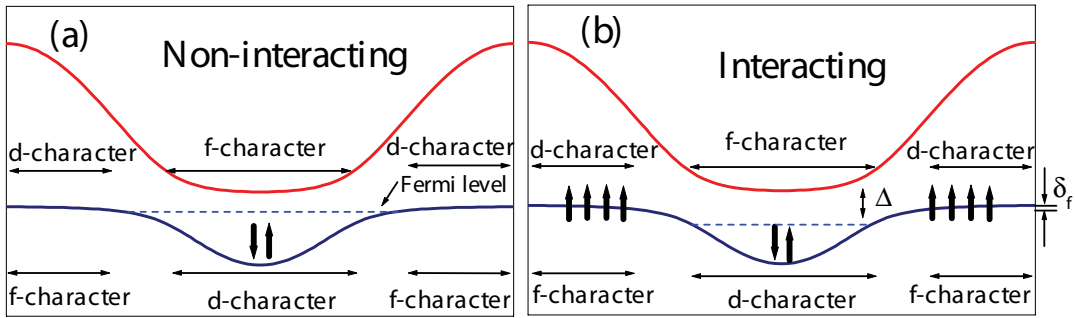


Figure 13: Schematic illustration of the segmented band character for a one-dimensional chain. (a) The energy occupancy for the non-interacting case; (b) the renormalization of the energy occupancy when the interaction is present [38].

scales Δ , the gap of the system, and δ , the energy cost of the spread of the electrons out of the Fermi sea into the f -like state. If $\Delta \gg \delta_f$, a ferromagnetic state will exist.

To assess the stability of the ferromagnetic state and the relevance of the model to real

materials, Batista *et al.* [39] added dispersion to the f -band for a few test cases and found that it could sometimes greatly change the ground state. Using the CPMC and ED methods, Shik *et al.* [90] investigated the matter further. They found that depending on the values of t_f and ε_f strong antiferromagnetism was induced among the f -electrons, but their ED results, for example, the third plot of Fig. 11, showed that positive dispersion and large negative dispersion seems to destroy the ferromagnetic ordering but the negative dispersion, when not too large, seems to enhance it for the given values of ε_f .

4.3 Falicov-Kimball model

Considerable numerical and analytic work has been poured into the original version of the Falicov-Kimball model [31]

$$H = -t_d \sum_{\langle i,j \rangle} (d_i^\dagger d_j + d_j^\dagger d_i) + \varepsilon_f \sum_i n_i^f + U \sum_i n_i^d n_i^f. \quad (4.2)$$

Besides conserving the total number $N = N_d + N_f$ of electrons, this Hamiltonian also conserves the number of d -electrons $N_d = \sum_i n_i^d$, the number of f -electrons $N_f = \sum_i n_i^f$, and the number of f -electrons n_i^f at each site. The latter conservation enables the rewriting of the Hamiltonian as

$$H' = -t_d \sum_{\langle i,j \rangle} (d_i^\dagger d_j + d_j^\dagger d_i) + \varepsilon_f \sum_i w_i + U \sum_i n_i^d w_i, \quad (4.3)$$

where the $w_i = 0$ or 1 are the eigenvalues of n_i^f constrained so that $N_f = \sum_i w_i$. Being quadratic in the creation and destruction operators, (4.3) has the form of a non-interacting problem. Accordingly, as the main numerical approach, a conventional eigensolver, a true exact diagonalization method, is used to find all the eigenvalues for each Hamiltonian representing one of the 2^L possible configurations of f -electrons for a lattice of L sites and a given value of N . When L gets too large, a Monte Carlo method is used to sample the most important configurations. By inspection, the configuration with the lowest total energy determines the ground state.

For one-dimensional systems, various types of charge-ordered, mixed valent, and phase-separated states are found as a function of the model's parameters and electron density [91–94]. A true exact diagonalization was used. Transitions between conducting and insulating states as well as valence transitions are observed. In contrast to Hartree-Fock predictions, the number of discrete valence transitions were found to be just a few for large U . In weak coupling, the valence transitions are gradual, metal-insulator-like, and accompanied by a discontinuous change in the energy gap. In strong coupling they are also metal-insulator-like. There are also relatively fewer phases and these are formed from the most homogeneous of possible configurations with the smallest periods.

The conservation of n_i^f implies the absence of f -electron dynamics

$$i\hbar \frac{dn_j^f}{dt} = [n_j^f, H] = 0.$$

This absence clearly restricts the physics of the model, and it is not surprising that when an on-site hybridization was added,

$$H = -t_d \sum_{\langle i,j \rangle} (d_i^\dagger d_j + d_j^\dagger d_i) + \varepsilon_f \sum_i n_i^f + U \sum_i n_i^d n_i^f + V \sum_i (d_i^\dagger f_i + f_i^\dagger d_i), \quad (4.4)$$

which breaks this symmetry (and the conservation of N_d and N_f), the physics markedly changed.

The most interesting physical consequence of such a symmetry breaking is a proposal by Sham and co-workers [44, 45] that when the on-site orbitals have opposite parity, a Hamiltonian such as

$$H = -t_d \sum_{\langle i,j \rangle} (d_i^\dagger d_j + d_j^\dagger d_i) + \varepsilon_f \sum_i n_i^f + U \sum_i n_i^d n_i^f + V \sum_{i,\nu=\hat{x},\hat{y}} (d_i^\dagger f_{i+\nu} + f_{i+\nu}^\dagger d_i - f_i^\dagger d_{i+\nu} - d_{i+\nu}^\dagger f_i) \quad (4.5)$$

can exhibit a ferroelectric ground-state caused by a Bose-Einstein condensation (BEC) of excitons (bound particle-hole pairs) accompanied by the spontaneous generation of an on-site hybridization which breaks spatial inversion symmetry.

In a series of papers, Farašovký [95–97] studied the role of local hybridization on the valence and metal-insulator transitions in the one- and two-dimensional versions of Eq. (4.4) by using the Lanczos and DMRG methods. Targeted were the gaps in the energy spectrum. He found that at zero hybridization the gaps in the d and f density of states do not coincide and almost all the f -electron spectral weight is located outside the d -electron sub-bands. For nonzero hybridization the d and f gaps coincide. No hybridization driven metal-insulator transitions were found in either dimension.

Farašovký also studied the effect of a non-local hybridization on these transitions in the one dimensional version of Eq. (4.5) by using the DMRG method [98, 99]. Significant differences between the results for local and non-local hybridizations occur. The effect of non-local hybridization can be so strong that it can induce a metal-insulator transition even in the 1/2-filled case where the ground states with and without hybridization are insulating for all finite values of the Coulomb interaction. This metallic state persists outside the 1/2-filled case and up to relatively large values of ε_f where the model undergoes a continuous transition into an insulating state.

The novel condensate proposal was also investigated numerically by Farašovky with the Lanczos methods [100] and then with the DMRG method [101], using Eq. (4.4) in one dimension with the on-site hybridization treated as a small symmetry breaking term. As V vanished the expectation value $\langle f_i^\dagger d_i \rangle$ vanished which was interpreted as signifying the absence of the proposed electronic ferroelectricity. Thus his conclusion is correct but trivial.

In a series of papers, Batista and co-workers [8–10] clarified the situation. Breaking the conservation of on-site f occupancy (but not the conservation of N_d and N_f) by starting

with

$$H = -t_d \sum_{\langle i,j \rangle} (d_i^\dagger d_j + d_j^\dagger d_i) + \varepsilon_d \sum_i n_i^d + U \sum_i n_i^d n_i^f - t_f \sum_{\langle i,j \rangle} (f_i^\dagger f_j + f_j^\dagger f_i) + \varepsilon_f \sum_i n_i^f \quad (4.6)$$

instead of Eq. (4.4) or (4.5), Batista [8] first showed that in the strong coupling limit ($U \gg |t_d|, |t_f|$) this Hamiltonian is equivalent to an anti-ferromagnetic spin-1/2 XXZ -Heisenberg model in an external magnetic field where the true electron spin operators are replaced by the pseudo-spin operators Eq. (3.13). From extensive pre-existing numerical work in two and three dimensions, this model is known to possess a state of planar magnetization (perpendicular to the pseudo z -direction) for a sufficiently strong pseudo-magnetic field. In this state the x -component of the pseudo-magnetization corresponds to a state of spontaneous global on-site hybridization, and the y -component, to a state of spontaneous ordering of local atomic currents, a magnetic quadrupolar state. The two component order parameter $M^\perp = (M^x, M^y) \rightarrow |M^\perp| e^{i\phi}$ exhibits the phase coherence of a condensate. Additionally, for weaker fields, the ground state is pseudo-antiferromagnetic, corresponding to a staggered ordering of atomic orbitals in terms of the original degrees of freedom.

The Lanczos and constrained-path Monte Carlo method were used to study Eq. (4.6) in the intermediate coupling regime and confirmed the persistence of the basic features of the strong coupling phase diagram. The nature of the ground state was determined by examining the pseudo-spin correlation functions and extrapolating their peaks to the thermodynamic limit. Figure 14 shows the one and two dimensional phase diagrams obtained with the CPMC method.

The effects of an off-site hybridization was next considered by using

$$\begin{aligned} H = & -t_d \sum_{\langle i,j \rangle} (d_i^\dagger d_j + d_j^\dagger d_i) + \varepsilon_d \sum_i n_i^d + U \sum_i n_i^d n_i^f \\ & + V \sum_{i,\nu=\hat{x},\hat{y}} (d_i^\dagger f_{i+\nu} + f_{i+\nu}^\dagger d_i - f_i^\dagger d_{i+\nu} - d_{i+\nu}^\dagger f_i) \\ & - t_f \sum_{\langle i,j \rangle} (f_i^\dagger f_j + f_j^\dagger f_i) + \varepsilon_f \sum_i n_i^f. \end{aligned} \quad (4.7)$$

Perturbation arguments, supported by Lanczos and constrained-path Monte Carlo calculations, proposed that the spontaneous hybridization of the orbitals, and hence a ferroelectric ground state, can still occur, but only $S^x(q=0)$ extrapolates to a non-zero value in the thermodynamic limit. This is illustrated in Fig. 15. Accordingly, the effect of the off-site hybridization is to change the ground state from one that breaks gauge invariance (breaks $U(1)$ symmetry) to one that breaks a polar symmetry (a Z_2 symmetry).

In the original Falicov-Kimball model (4.2), the conservation of local f -electron charge corresponds to a local gauge symmetry: $f_i^\dagger \rightarrow e^{i\phi} f_i^\dagger$. The phase coherent condensate represented by the BEC of excitons corresponds to the breaking of a global gauge symmetry. By Elitzur's Theorem [102], a global gauge symmetry cannot be broken if a local gauge

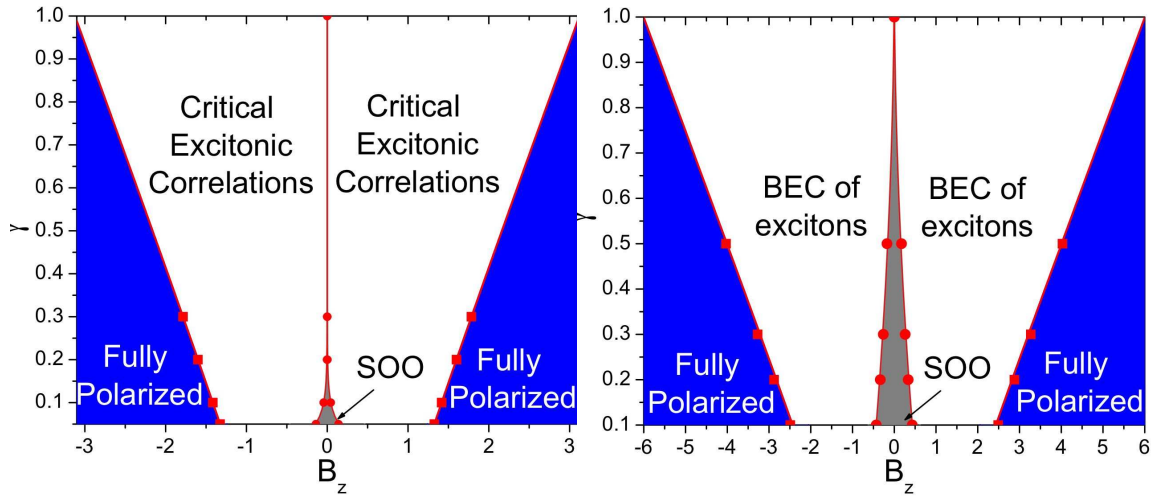


Figure 14: On the left and right are the one and two dimensional phase diagrams of the version of the Falicov-Kimball model described by Eq. (4.6). Here, $B_z = \varepsilon_d - \varepsilon_f$, SOO denotes staggered orbitally ordered, and fully polarized refers all the d or f orbitals being fully occupied at each lattice site [9].

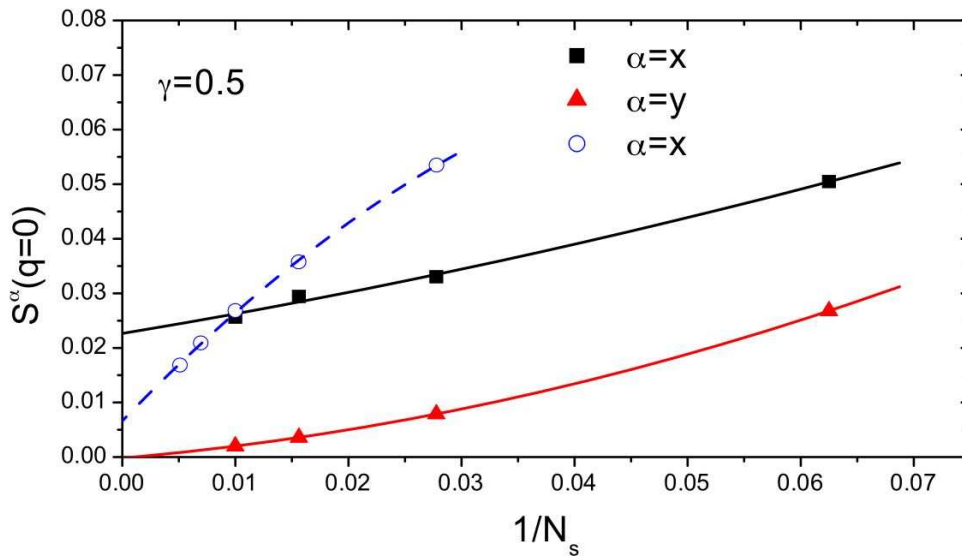


Figure 15: Extrapolation of the pseudospin correlation functions to the thermodynamic limit for a two-dimensional Falicov-Kimball model (4.7) with off-site hybridization. The dashed curve for the x -component is for $U = 2$; the others are for $U = 4$ [9].

symmetry exists. Physically, the holes cannot move, and hence cannot condense. To allow the necessary dynamics, the local gauge symmetry has to be eliminated. The sequence of Hamiltonians, Eqs. (4.4) to (4.7) represents various ways of doing this, but only Eq. (4.6) leads to BEC. Mean-field theory predicts a BEC of excitons as a ground state for Eq. (4.5).

Adding spin is the next natural enhancement to the Falicov-Kimball model [95]. There are several ways to do this, leading to several generalizations of the Falicov-Kimball model that are special cases of a two-band Hubbard model

$$H = - \sum_{\langle i,j \rangle, \nu, \nu', \sigma} t_{\nu\nu'} \left(c_{i\nu\sigma}^\dagger c_{j\nu'\sigma} + c_{j\nu'\sigma}^\dagger c_{i\nu\sigma} \right) + \sum_{i, \nu} \varepsilon_\nu n_i^\nu + \sum_i U_{df} n_i^d n_i^f + \sum_{i, \nu} U_{\nu\nu} n_{i\uparrow}^\nu n_{i\downarrow}^\nu, \quad (4.8)$$

where $\nu = \{d, f\}$, $c_{i\nu\sigma}^\dagger = \{d_{i\sigma}^\dagger, f_{i\sigma}^\dagger\}$, $n_{i\sigma}^\nu = c_{i\nu\sigma}^\dagger c_{i\nu\sigma}$, and $n_i^\nu = \sum_\sigma n_{i\sigma}^\nu$.

Using a true exact diagonalization method, the Lanczos method, and small clusters, Farašovsky and coworkers [103–105] studied cases of this Hamiltonian that conserved $n_{i\sigma}^f$. The focus was on the consequence of a U_{df} in the absence of an interband hybridization. One- and two-dimensional lattices were studied. Typically U is very large. They found that their models describe two types of discontinuous valence transitions: In the weak coupling limit there is a metal-insulator transition from an integer valence state with $n_f = 1$ to a mixed valence state with $0 < n_f < 1$; in the strong coupling limit there is a metal-insulator transition from $n_f = 1$ to $n_f = 0$. The detailed picture is relatively complicated. Phase-separated states were also found. Some evidence of pairing of local f -electrons was also reported.

Batista and coworkers [106] analytically studied Eq. (4.8) in the strong coupling limit and proved that ferromagnetism and ferroelectricity can co-exist in the ground state in the limit $U_{aa}, U_{bb} \rightarrow \infty$. They then used the Lanczos method to compute the strong coupling phase diagram for a small cluster. A rich variety of co-existing phases was seen. Equation (4.8) is presently being investigated by the DMRG and constrained path Monte Carlo methods for larger lattices at weaker couplings.

Some other work on the Falicov-Kimball model includes changing the nearest neighbor hopping to being long ranged [107, 108] or correlated (dependent on the occupancy of the f -orbitals at the two sites) [109–111]. The consequences relative to the original Falicov-Kimball model can be significant, for example, inducing metal-insulator transitions where there were previously none. We will not discuss these results further.

5 Summary

Numerical studies have revealed a variety of ground state behaviors for the three-band Hubbard, periodic Anderson, and Falicov-Kimball models. Some of the behaviors were expected; some were not. These methods are clearly a valuable tool for unravelling and unveiling the fascinating consequences that quantum mechanics has on the properties of systems of interacting electrons.

For the three-band Hubbard model, the numerical results point to ground states where holes bind. The expected consequences of this binding, phase separation or superconductivity, remain underestablished. A superconducting state, if it exists, is likely extremely

subtle, as the vertex contribution to the pairing correlations, that is, the part due to the dressing of the electron by the interactions, is small and appears to scale into the noise of the simulation as the lattice size or interaction strength is increased. The static spin structure factor sometimes exhibits features consistent with experiment, but such features are possibly a general consequence of spin fluctuations rather than a signature of an incipient superconducting state [112].

Perhaps the most surprising finding for the periodic Anderson model is the apparent minor role played by the competition between the RKKY and Kondo interactions in framing most of its physics. The now well-established itinerant ferromagnetic region is novel in that at least three different mechanisms have been documented for its origin. Its most striking feature is the co-existence of itinerant ferromagnetism and mixed valency. This co-existence is in sharp contrast to the predictions of many mean-field theories. While the different mechanisms appear in different parameters regimes, their common physics are constructive quantum interference effects. The observed itinerant magnetism is definitely more Nagaoka-like than Stoner-like [40, 114].

Metallic to insulating transitions are found in various types of the Falicov-Kimball models. The novel purely electronic mechanism for ferroelectricity is now well established and clarified. Along with this is the appreciation that the dynamics of the f -electrons, absent in the original model, is essential to this physics. Multiferroric behavior is now being simulated more extensively in generalizations of the model.

These results and others point to the strength of the numerical methods used. An important point is that while the Monte Carlo methods have not pulled superconductivity out of the three-band model, they have pulled a non-trivial phase coherent ground state out of an extended Falicov-Kimball model. This state of off-diagonal long-range order co-exists with an ordered state of atomic currents.

The numerical methods are not without their shortcomings. The Lanczos method is restricted to small systems, the density-matrix renormalization group is best in one dimension and short-ranged interactions, and quantum Monte Carlo methods, such as the constrained-path method, have limited precision. The limitations in the Lanczos method are intrinsic; those for the other two are less so. As an agenda for future research, attention to algorithmic improvement is encouraged. An area needing the most attention is finite temperature methods.

In short, multiband models present an opportunity to explore and discover novel physical phenomena and yet remain simple enough so the interpretation of this physics is possible. Various numerical methods are an important tool toward researching this physics. The current interest of multiband models is poised to grow.

Acknowledgments

This work was supported in part by the Earmarked Grant for Research from the Research Grants Council (RGC) of the HKSAR, China (Project CUHK 401703). The work of JEG

was supported by the US Department of Energy. We thank C. D. Batista for several helpful suggestions regarding the manuscript. HQL also acknowledges useful discussions with D. S. Wang and hospitality of Institute of Physics, CAS, through grant NSFC 10329403.

References

- [1] G. H. Golub and C. F. van Loan, *Matrix Computations*, Johns Hopkins University Press, Baltimore, 1989.
- [2] S. Pissanetsky, *Sparse Matrix Technology*, Academic Press, London, 1984.
- [3] S. R. White, Density matrix formulation for quantum renormalization groups, *Phys. Rev. Lett.*, 69 (1992), 2863-2866.
- [4] E. Y. Loh, Jr., J. E. Gubernatis, R. T. Scalettar, S. R. White, D. J. Scalapino and R. L. Sugar, Sign problem in the numerical simulation of many-electron systems, *Phys. Rev. B*, 41 (1990), 9301-9307.
- [5] S. Zhang, J. Carlson and J. E. Gubernatis, Constrained path quantum Monte Carlo method for fermion ground states, *Phys. Rev. Lett.*, 74 (1995), 3652-3655.
- [6] S. Zhang, J. Carlson and J. E. Gubernatis, Constrained path Monte Carlo method for fermion ground states, *Phys. Rev. B*, 55 (1997), 7464-7477.
- [7] J. Carlson, J. E. Gubernatis, G. Ortiz and S. Zhang, Issues and observations on applications of the constrained-path Monte Carlo method to many-fermion systems, *Phys. Rev. B*, 59 (1999), 12788-12798.
- [8] C. D. Batista, Electronic ferroelectricity in the Falicov-Kimball model, *Phys. Rev. Lett.*, 89 (2002), 166403-166406.
- [9] C. D. Batista, J. E. Gubernatis, J. Bonca and H. Q. Lin, Intermediate coupling theory of electronic ferroelectricity, *Phys. Rev. Lett.*, 92 (2004), 187601-187604.
- [10] J. Bonca, C. D. Batista, J. E. Gubernatis and H. Q. Lin, Electronically driven ferroelectricity in the extended Falicov-Kimball model, *Int. J. Mod Phys B*, 19 (2005), 525-527.
- [11] H. Q. Lin and J. E. Gubernatis, Exact diagonalization methods for quantum systems, *Comput. Phys.*, 7 (1993), 400-407.
- [12] U. Schollwöck, The density-matrix renormalization group, *Rev. Mod. Phys.*, 77 (2005), 259-315.
- [13] J. Hubbard, Electron correlations in narrow energy bands, *Proc. R. Soc. London, Ser. A*, 276 (1963), 238-258.
- [14] F. C. Zhang and T. M. Rice, Effective Hamiltonian for the superconducting Cu oxides, *Phys. Rev. B*, 37 (1988), 3759-3761.
- [15] E. R. Davidson, Monster matrices: Their eigenvalues and eigenvectors, *Comput. Phys.*, 7 (1993), 519-522.
- [16] R. M. Noack and S. R. Manmana, Diagonalization and numerical renormalization-group-based methods for interacting quantum system, *AIP Conf. Proc.*, 789 (2005) 93-163.
- [17] S. R. White, Density matrix renormalization group algorithms with a single center site, *cond-mat/0508709*.
- [18] S. Sorella, S. Baroni, R. Car and M. Parrinello, A novel technique for the simulation of interacting fermion systems, *Europhys. Lett.*, 8 (1989), 663-668.
- [19] S. R. White, D. J. Scalapino, R. L. Sugar, E. Y. Loh, Jr., J. E. Gubernatis and R. T. Scalettar, Numerical study of the two-dimensional Hubbard model, *Phys. Rev. B*, 40 (1989), 506-516.
- [20] H. J. M. van Bommel, D. F. B. ten Haaf, W. van Saarloos, J. M. J. van Leeuwen and G. An, Fixed-node quantum Monte Carlo method for lattice fermions, *Phys. Rev. Lett.*, 72 (1994),

2442-2445.

- [21] M. Kalos and P. Whitlock, Monte Carlo methods I: basics, John Wiley, New York, 1986.
- [22] N. Metropolis, A. W. Rosenbluth, M. N. Rosenbluth, A. H. Teller and E. Teller, Equation of state calculations by fast computing machines, *J. Phys. Chem.*, 21 (1953), 1087-1092.
- [23] M. Suzuki, General decomposition theory of exponential operators, in: *Quantum Monte Carlo Methods in Condensed Matter physics*, World Scientific Press, Singapore, 1993.
- [24] J. E. Hirsch, Two-dimensional Hubbard model: Numerical simulation study, *Phys. Rev. B*, 31 (1985), 4403-4419.
- [25] J.-P. Blaizot and G. Ripka, *Quantum Theory of Finite-systems*, MIT Press, Cambridge, 1985.
- [26] A. C. Cosentini, M. Capone, L. Guidoni and G. B. Bachelet Phase separation in the two-dimensional Hubbard model: a fixed-node quantum Monte Carlo study, *Phys. Rev. B*, 58 (1998), R14685-R14688.
- [27] D. F. B. ten Haaf, H. J. M. van Bemmelen, J. M. J. van Leeuwen, W. van Saarloos and D. M. Ceperley, Proof for an upper bound in fixed-node Monte Carlo for lattice fermions, *Phys. Rev. B*, 51 (1995), pp. 13039-13045.
- [28] J. Hubbard, Electron correlation in narrow energy bands, *Proc. Roy. Soc.*, A276 (1963), 238-257.
- [29] M. C. Gutzwiller, Effect of correlation on ferromagnetism of transition metals, *Phys. Rev. Lett.*, 10 (1963), 159-162.
- [30] V. J. Emery, Theory of high- T_c superconductivity in oxides, *Phys. Rev. Lett.*, 58 (1987), 2794-2797.
- [31] L. M. Falicov and J. C. Kimball, Simple model for semiconductor-metal transitions: SmB_6 and transition-metal oxides, *Phys. Rev. Lett.*, 22 (1969), 997-999.
- [32] R. T. Scalettar, Magnetic and pairing correlations in a three-band Hubbard model, *Physica C*, 162-164 (1989), 313-318.
- [33] G. Dopf, A. Muramatsu and W. Hanke, 3-band Hubbard model - a Monte-Carlo study, *Phys. Rev. B*, 41 (1990), 9264-9276.
- [34] S. R. White, D. J. Scalapino, R. L. Sugar, N. E. Bickers and R. T. Scalettar, Attractive and repulsive pairing interaction vertices for the two-dimensional Hubbard model, *Phys. Rev. B*, 39 (1989), 839-842.
- [35] D. W. Hess, P. S. Riseborough and J. L. Smith, *Ency. Appl. Phys.*, 7 (1993), p. 435.
- [36] M. Guerrero and R. M. Noack, Ferromagnetism and phase separation in one-dimensional d-p and periodic Anderson models, *Phys. Rev. B*, 63 (2001), 144423-144423.
- [37] C. D. Batista, J. Bonca and J. E. Gubernatis, Ferromagnetism in the two-dimensional periodic Anderson model, *Phys. Rev. B*, 63 (2001), 184428-184440.
- [38] C. D. Batista, J. Bonca and J. E. Gubernatis, Segmented band mechanism for itinerant ferromagnetism, *Phys. Rev. Lett.*, 88 (2002), 187203-187206.
- [39] C. D. Batista, J. Bonca and J. E. Gubernatis, Itinerant ferromagnetism in the periodic Anderson model, *Phys. Rev. B*, 68 (2003), 214430-214442.
- [40] C. D. Batista, J. Bonca and J. E. Gubernatis, Ferromagnetism in the strong hybridization regime of the periodic Anderson model, *Phys. Rev. B*, 68 (2003), 64403-64406.
- [41] P. Fulde, J. Keller and G. Zwicknagl, *Solid State Physics* 41, Academic, New York, 1990.
- [42] S. Schwieger and W. Nolting, Stabilization of d-band ferromagnetism by hybridization with uncorrelated bands, *Phys. Rev. B*, 64 (2001), 144415-144422.
- [43] T. Kennedy and E. H. Lieb, An itinerant electron model with crystalline or magnetic long-range order, *Physica A*, 138 (1986), 320-358.
- [44] T. Portengen, T. Östreich and L. J. Sham, Linear and nonlinear optical characteristics of the

- Falicov-Kimball model, Phys. Rev. Lett., 76 (1996), 3384-3387.
- [45] T. Portengen, T. Östreich and L. J. Sham, Theory of electronic ferroelectricity, Phys. Rev. B, 54 (1996), 17452-17463.
- [46] R. T. Scalettar, D. J. Scalapino, R. L. Sugar and S. R. White, Antiferromagnetic, charge-transfer, and pairing correlations in the 3-band Hubbard model, Phys. Rev. B, 44 (1991), 770-781.
- [47] G. Dopf, A. Muramatsu and W. Hanke, Consistent description of high- T_c superconductors with the 3-band Hubbard model, Phys. Rev. Lett., 68 (1992), 353-356.
- [48] G. Dopf, J. Wagner, P. Dieterich, A. Muramatsu, and W. Hanke, Single-particle spectrum for high- T_c superconductors - a numerical study, Helv. Phys. Acta, 65 (1992), 431-432.
- [49] G. Dopf, A. Muramatsu and W. Hanke, Antiferromagnetism and incommensurate structure in the 3-band Hubbard model, Europhys. Lett., 17 (1992), 559-564.
- [50] Masao Ogata and Hiroyuki Shiba, Holes in two-dimensional CuO_2 system - pairing mechanism emerging from small-cluster studies, J. Phys. Soc. Jpn., 57 (1988), 3074-3088.
- [51] J. E. Hirsch, S. Tang, E. Loh Jr. and D. J. Scalapino, Pairing interaction in two-dimensional CuO_2 , Phys. Rev. Lett., 60 (1988), 1668-1671.
- [52] J. E. Hirsch, S. Tang, E. Loh Jr. and D. J. Scalapino, Pairing interaction in CuO clusters, Phys. Rev. B, 39 (1989), 243-253.
- [53] W. H. Stephan, W. von der Linden and P. Horsch, Attractive interactions from repulsive forces in a multiband Hubbard model, Phys. Rev. B, 39 (1989), 2924-2927.
- [54] M. Frick, P. C. Pattnaik, I. Morgenstern, D. M. Newns and W. von der Linden Monte Carlo study of superconductivity in the three-band Emery model, Phys. Rev. B, 42 (1990), 2665-2668.
- [55] K. Kuroki and H. Aoki, Quantum Monte Carlo evidence for superconductivity in the three-band Hubbard model in two dimensions, Phys. Rev. Lett., 76 (1996), 4400-4403.
- [56] H. Endres, W. Hanke, H. G. Evertz and F. F. Assaad, Quantum Monte Carlo evidence for superconductivity in the three-band Hubbard model in two dimensions, Phys. Rev. Lett., 78 (1997), 160-160.
- [57] K. Kuroki and H. Aoki, Quantum Monte Carlo evidence for superconductivity in the three-band Hubbard model in two dimensions - reply, Phys. Rev. Lett., 78 (1997), 161-161.
- [58] M. Guerrero, J. E. Gubernatis and S. W. Zhang, Quantum Monte Carlo study of hole binding and pairing correlations in the three-band Hubbard model, Phys. Rev. B, 57 (1998), 11980-11988.
- [59] Z. B. Huang, H. Q. Lin and J. E. Gubernatis, Pairing, charge, and spin correlations in the three-band Hubbard model, Phys. Rev. B, 63 (2001), 115112-115121.
- [60] Daniel Duffy and Adriana Moreo, Influence of next-nearest-neighbor electron hopping on the static and dynamical properties of the two-dimensional Hubbard model, Phys. Rev. B, 52 (1995), 15607-15616.
- [61] Charles Buhler and Adriana Moreo, Spin and charge fluctuations in the U-t-t' model, Phys. Rev. B, 59 (1999), 9882-9887.
- [62] Z. B. Huang, H. Q. Lin and J. E. Gubernatis, Quantum Monte Carlo study of spin, charge, and pairing correlations in the t-t'-U Hubbard model, Phys. Rev. B, 64 (2001), 205101-25110.
- [63] T. E. Mason, G. Aeppli, S. M. Haydeu, A. P. Hamiver and H. A. Mook, Low energy excitations in superconducting $La_{1.86}Sr_{0.14}CuO_4$, Phys. Rev. Lett., 71 (1993), 919-922.
- [64] R. Blankenbecler, J. R. Fulco, W. Gill and D. J. Scalapino, Ground-state properties of the periodic Anderson model, Phys. Rev. Lett., 58 (1987), 411-414.
- [65] P. K. Misra, D. G. Kanhere and J. Callaway, Periodic Anderson model for 4-site clusters,

- Phys. Rev. B, 35 (1987), 5013-5024.
- [66] J. Callaway, D. P. Chen, D. G. Kanhere and P. K. Misra, Cluster simulation of the lattice Anderson model, Phys. Rev. B, 38 (1988), 2583-2595.
 - [67] K. Ueda, Numerical diagonalization of the periodic Anderson model ground-state and magnetization process, J. Phys. Soc. Jpn., 58 (1989), 3465-3468.
 - [68] Y. Zhang and J. Callaway, Monte-Carlo simulations of the Periodic Anderson model on a square lattice, Phys. Rev. B, 38 (1988), 641-645.
 - [69] J. Callaway, D. G. Kanhere and H. Q. Lin, Small cluster studies of the lattice Anderson model, J. Appl. Phys., 73 (1993), 5406-5408.
 - [70] J. Callaway, J. W. Kim, L. Tan and H. Q. Lin, Exact-diagonalization study of the spectral-weight functions and the density-of-states of the lattice Anderson model, Phys. Rev. B, 48 (1993), 11545-11552.
 - [71] J. Callaway, J. W. Kim, L. Tan, H. Q. Lin and H. Chen, Exact diagonalization studies of the lattice Anderson Model on a 4-site cluster, Physica B, 199 (1994), 316-318.
 - [72] H. Q. Lin, H. Chen and J. Callaway, Magnetic properties of the lattice Anderson model, J. Appl. Phys., 75 (1994), 7041-7043.
 - [73] K. Ueda, H. Tsunetsugu and M. Sigrist, Singlet ground-state of the periodic Anderson Model at half filling - a rigorous result, Phys. Rev. Lett., 68 (1992), 1030-1033.
 - [74] G. S. Tian, Antiferromagnetic order in the periodic Anderson Model at half filling - a rigorous result, Phys. Rev. B, 50 (1994), 6246-6249.
 - [75] C. Noce and M. Cuoco, Rigorous results for the one-dimensional symmetric Anderson model, Phys. Rev. B, 54 (1996), 11951-11952.
 - [76] T. Nishino and K. Ueda, Spin-excitation and charge-excitation gaps in the one-dimensional periodic Anderson model, Phys. Rev. B, 47 (1993), 12451-12458.
 - [77] G. S. Tian, Charge and spin-excitation gaps in half-filled strongly correlated electron systems: a rigorous result, Phys. Rev. B, 58 (1998), 7612-7618.
 - [78] G. S. Tian and L. H. Tang, General result on charge and spin-excitation gaps in strongly correlated electron systems at half filling, Phys. Rev. B, 60 (1999), 11336-11344.
 - [79] M. Guerrero and C. C. Yu, Kondo insulators modeled by the one-dimensional anderson lattice - a numerical-renormalization-group study, Phys. Rev. B, 51 (1995), 10301-10312.
 - [80] M. Guerrero and H. M. Carruzzo, Effect of dispersion in the f band of the one-dimensional Anderson lattice model, Phys. Rev. B, 54 (1996), 16562-16573.
 - [81] J. Bonca and J. E. Gubernatis, Effects of doping on spin correlations in the periodic Anderson model, Phys. Rev. B, 58 (1998), 6992-7001.
 - [82] B. Moller and P. Wolffe, Magnetic order in the periodic Anderson model, Phys. Rev. B, 48 (1993), 10320-10326.
 - [83] G. Kotliar and A. E. Ruckenstein, New functional integral approach to strongly correlated Fermi system: Gutzwiller approximation as a saddle point, Phys. Rev. Lett., 57 (1986), 1362-1365.
 - [84] M. Guerrero and R. M. Noack, Phase diagram of the one-dimensional Anderson lattice, Phys. Rev. B, 53 (1996), 3707-3712.
 - [85] Y. Q. Wang, Long Range Order in Strongly Correlated Systems, PhD Thesis, The Chinese University of Hong Kong, 2005.
 - [86] D. Meyer and W. Nolting, Periodic Anderson model: magnetic properties, Physica B, 281 (2000), 189-190.
 - [87] D. Meyer and W. Nolting, Dynamical mean-field study of ferromagnetism in the periodic Anderson model, Phys. Rev. B, 62 (2000), 5657-5666.

- [88] P. Santini, L. C. Andreani and H. Beck, Magnetic correlations in the Anderson lattice - an exact-diagonalization study, *Phys. Rev. B*, 47 (1993), 1130-1133.
- [89] H. Q. Lin, H. Y. Shik, Y. Q. Wang, C. D. Batista and J. E. Gubernatis, Investigating magnetic properties by quantum Monte Carlo simulations, *J. Magn. Magn. Matr.*, 281 (2004), 240-246.
- [90] H. Y. Shik, Y. Q. Wang, J. E. Gubernatis and H. Q. Lin, Effect of f-band dispersion on the magnetic properties of periodic Anderson lattice model, *J. Appl. Phys.*, 95 (2004), 7195-7197.
- [91] P. Farkasovsky, Falicov-Kimball model and the problem of valence and metal-insulator transitions, *Phys. Rev. B*, 51 (1995), 1507-1512.
- [92] P. Farkasovsky, Pressure-induced insulator-metal transitions in the spinless Falicov-Kimball model, *Phys. Rev. B*, 52 (1995), R5463-R5466.
- [93] S. Gal, The spinless Falicov-Kimball model away from half filling, *Mod. Phys. Lett. B*, 13 (1999), 515-522.
- [94] S. Gal, The ground-state phase diagram of the spinless 1D Falicov-Kimball model: numerical studies, *Czech. J. Phys.*, 49 (1999), 1105-1113.
- [95] P. Farkasovsky, The role of hybridization on valence transitions in the spinless Falicov-Kimball model, *Z. Phys. B-Condensed Matter*, 104 (1997), 553-557.
- [96] P. Farkasovsky, Influence of hybridization on ground-state properties of the Falicov-Kimball model, *Phys. Rev. B*, 65 (2002), 245119-245203.
- [97] P. Farkasovsky, The spectral properties of the Falicov-Kimball model in the weak-coupling limit, *Int. J. Mod. Phys. B*, 17 (2003), 2083-2093.
- [98] P. Farkasovsky, Effects of nonlocal hybridization on valence and metal-insulator transitions in the Falicov-Kimball model, *Phys. Rev. B*, 70 (2004), 035117-035202.
- [99] P. Farkasovsky, The influence of nonlocal hybridization on ground-state properties of the Falicov-Kimball model, *Physica B*, 359 (2005), 687-689.
- [100] P. Farkasovsky, Existence of a ferroelectric ground state with a spontaneous polarization in the Falicov-Kimball model, *Phys. Rev. B*, 59 (1999), 9707-9709.
- [101] P. Farkasovsky, Falicov-Kimball model and the problem of electronic ferroelectricity, *Phys. Rev. B*, 65 (2002), 081102-081105.
- [102] C. Itzykson and J.-M. Drouffe, *Statistical Field Theory*, Cambridge University, Cambridge, 1989.
- [103] P. Farkasovsky, Electronic phase transitions in the spin-1/2 Falicov-Kimball model, *Phys. Rev. B*, 54 (1996), 11261-11264.
- [104] P. Farkasovsky, Phase separation and metal-insulator transitions in the spin-1/2 Falicov-Kimball model, *Phys. Rev. B*, 60 (1999), 10776-10781.
- [105] P. Farkasovsky and H. Cencarikova, Ground states of the generalized Falicov-Kimball model in one and two dimensions, *Eur. Phys. J. B*, 47 (2005), 517-526.
- [106] C. D. Batista, J. E. Gubernatis and W.-G. Yin, Electronic mechanism for the coexistence of ferroelectricity and ferromagnetism, *cond-mat/0508113*.
- [107] P. Farkasovsky, The influence of hopping on valence transitions in the Falicov-Kimball model, *J. Phys.-Condensed Matter*, 7 (1995), 3001-3012.
- [108] P. Farkasovsky, Insulator-metal transitions in the Falicov-Kimball model with a generalized type of hopping, *J. Phys.-Condens. Matter*, 7 (1995), 9775-9783.
- [109] P. Farkasovsky and S. Gal, Electronic phase transitions in the spinless Falicov-Kimball model with correlated hopping, *Phase Transit.*, 74 (2001), pp. 375-389.
- [110] P. Farkasovsky and N. Hudakova, Ground-state properties of the Falicov-Kimball model with correlated hopping in two dimensions, *J. Phys.-Condensed Matter*, 14 (2002), 499-506.
- [111] H. Cencarikova and P. Farkasovsky, Ground states of the two-dimensional Falicov-Kimball

- model with correlated hopping, *Physica B*, 359 (2005), 690-692.
- [112] C. D. Batista, G. Ortiz and A. V. Balatsky, Unified description of the resonance peak and incommensuration in high- T_c superconductors, *Phys. Rev. B*, 64 (2001), 172508-172511.
 - [113] C. D. Batista, J. Bonca and J. E. Gubernatis, Ferromagnetism in the strong hybridization regime of the periodic Anderson model, *Phys. Rev. B*, 68 (2003), 064403-064406.
 - [114] C. D. Batista and J. E. Gubernatis, unpublished.